2019 Fall

"Advanced Physical Metallurgy"

- Non-equilibrium Solidification -

11.12.2019

Eun Soo Park

Office: 33-313
Telephone: 880-7221
Email: espark@snu.ac.kr
Office hours: by appointment

4.6 Bulk Metallic Glass Casting Methods

4.6.1 Water-Quenching Method : CR~ about 10-100 K/s

4.6.2 High-Pressure Die Casting

: offer high solidification rates high productivity, low casting defect, and possible to produce more complex shapes even in alloys with a high viscosity

4.6.6 Squeeze-casting Method

: Push the molten alloy through hydraulic high pressure into the Cu mold until the liquid alloy completely solidified → Undercooling to much below the equilibrium solidification temperature

4.6.3 Copper Mold Casting : most common and popular method to produce BMGs

: Injection casting, Centrifugal casting, Strip casting, Arc melting, Suction casting, tilt-casting, Cap-cast technique (bringing a metallic cap into contact with the molten metal, and applied a small pressure of about 1 kN → high CR)

→ **Automatic Production Process of BMGs (Human error ↓ & Homogeneity ↑)**

4.6.8 Unidirectional Zone Melting Method

4.6.9 Electromagnetic Vibration Process

: destroy clusters of strong local order → GFA↑

4.8 Mechanical Alloying → Extrusion or Spark Plasma Sintering (multi-step process)

: used to easily produce amorphous phases in those systems where conventional melting and casting methods prove difficult or impossible (wide composition ranges)

4.7 Bulk Metallic Glass Composites

: exhibit much better mechanical properties → detail later in Chapter 8

The BMG composites have been designated as *in situ* or *ex situ* composites depending on the way these have been obtained. In the *in situ* composites, the second phase precipitates out of the metallic glass either during casting or subsequent processing of the fully glassy alloy. Accordingly, the interface between the glassy matrix and the crystalline reinforcement is very strong. On the other hand, in the *ex situ* method, the reinforcement phase is added separately during the casting/processing of the alloy and stays "as-is" without much interaction with the matrix. Consequently, the interface between the matrix and the reinforcement may not be very strong. Further, the volume fraction of the reinforcement phase is smaller in the *in situ* method and could be much higher in the *ex situ* method.

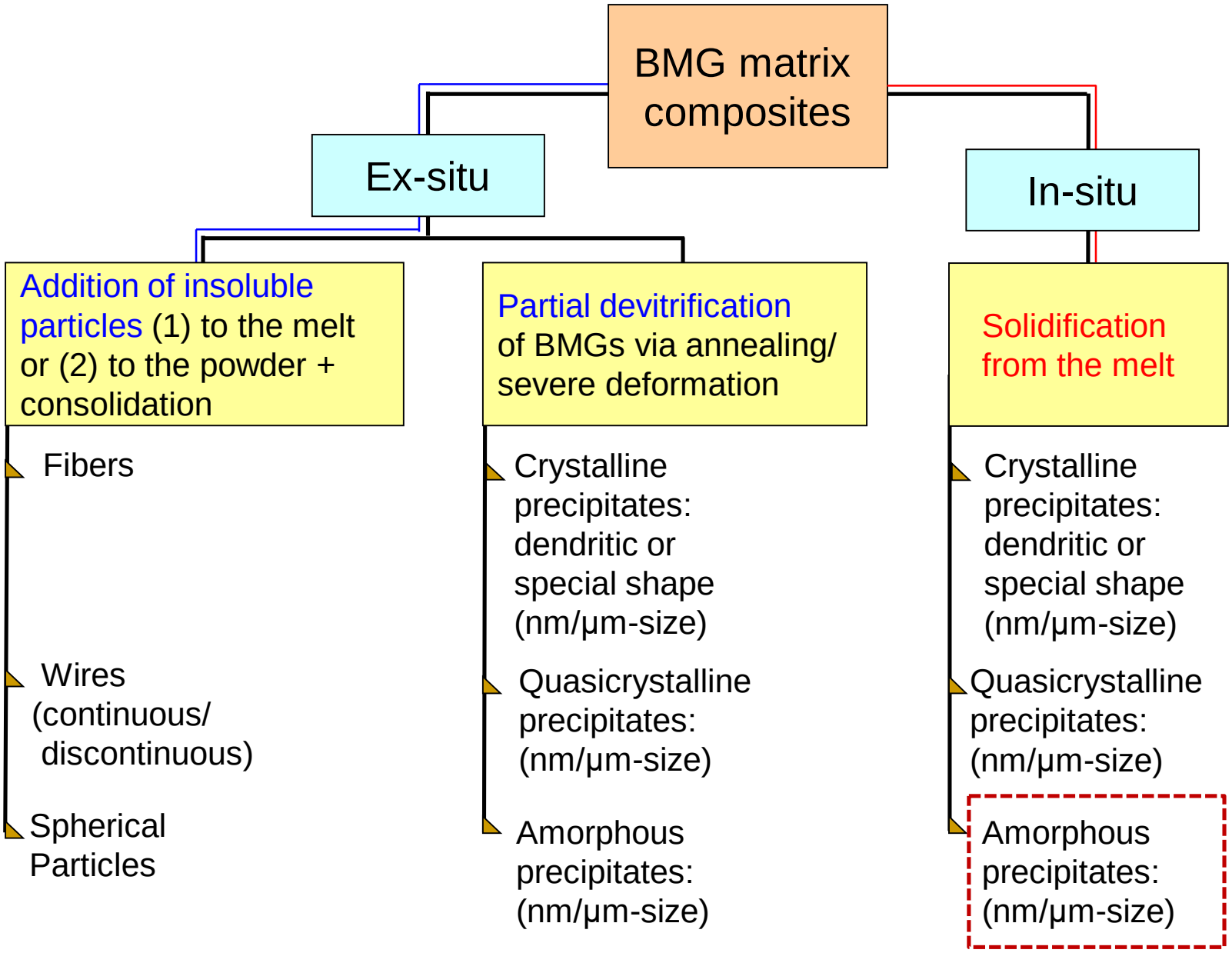

Eckert at al, Adv Eng Mater 2007

In-situ Composite

*Formation of a composite microstructure within a **single production step***

a), b) Crystalline precipitates

c) Quasicystalline precipitates

d) Two phase amorphous composites

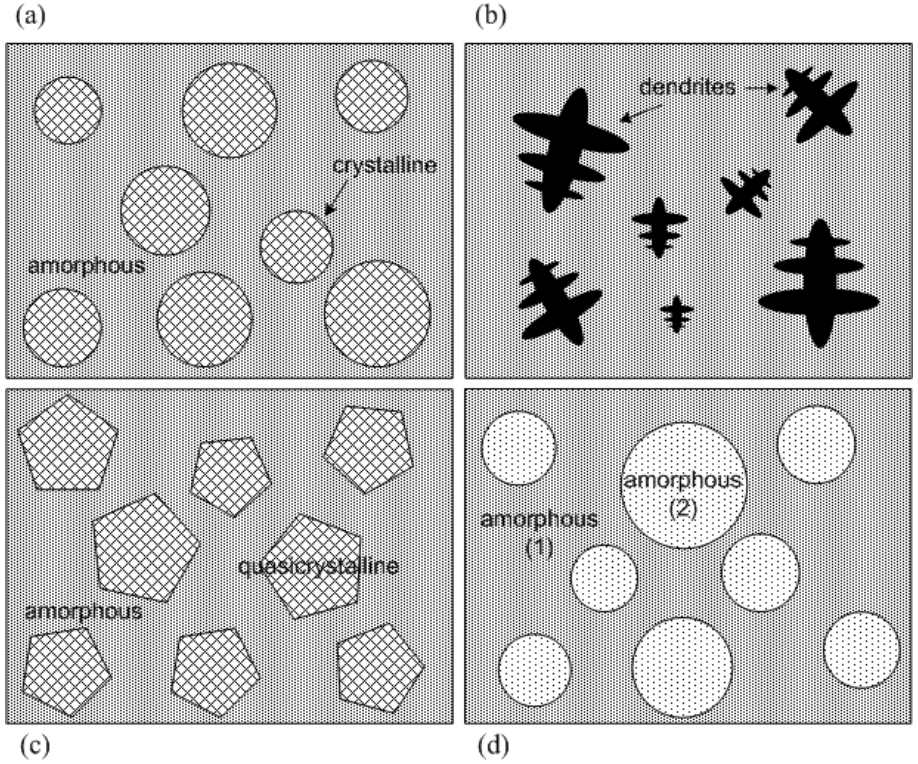

4.7.1 In Situ Composites: usually produced by adjusting the chemical composition of the alloy

: Shape of crystalline phase_usually dendritic → homogenized in the mushy (liquid+ soild) region_spherical shape → further improve the mechanical properties

1) Solidification : preciipitation of primary ductile phase

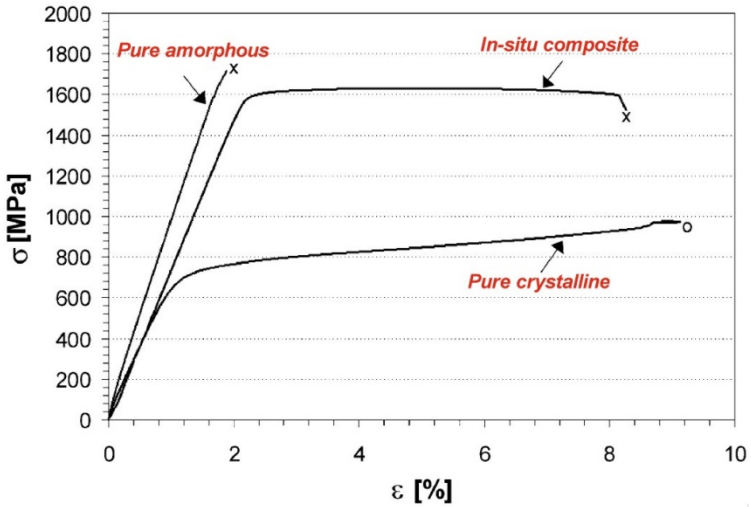

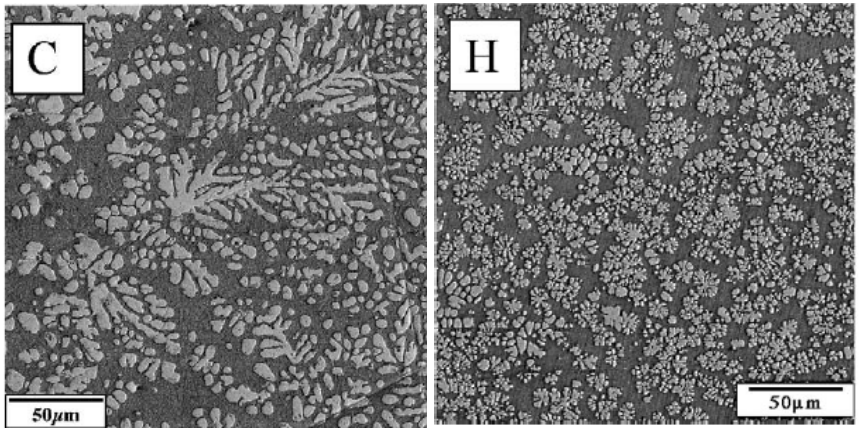

(Johnson et al., Acta Mater., 2001)

2) Solidification : precipitation of ductile phase

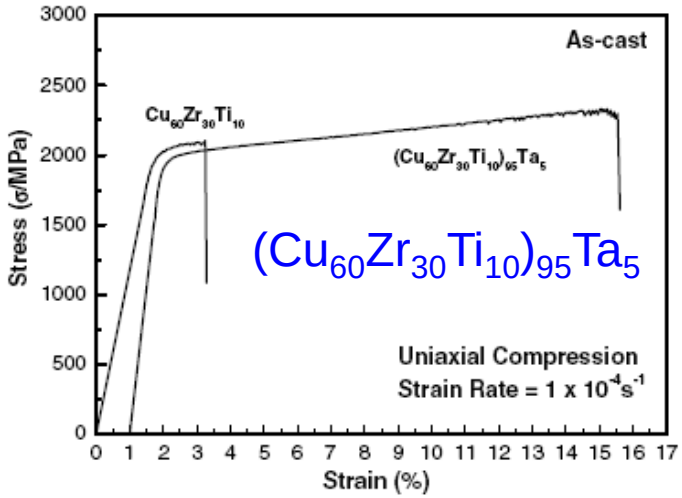

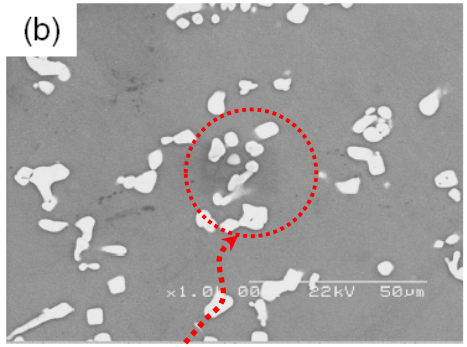

Ta rich particle

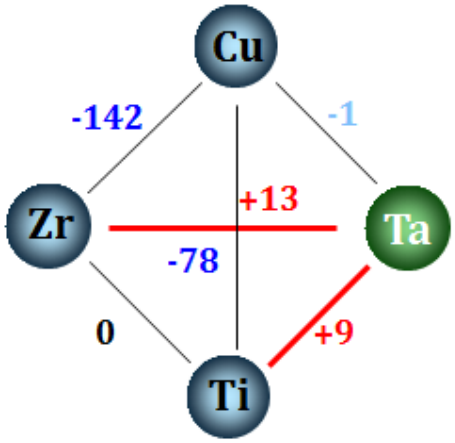

(Johnson et al., Acta Mater., 2001)

Shape Memory Bulk Metallic Glass Composites

Glass-forming and shape memory metals may provide a route to fabricating materials with enhanced mechanical properties.

Douglas C. Hofmann

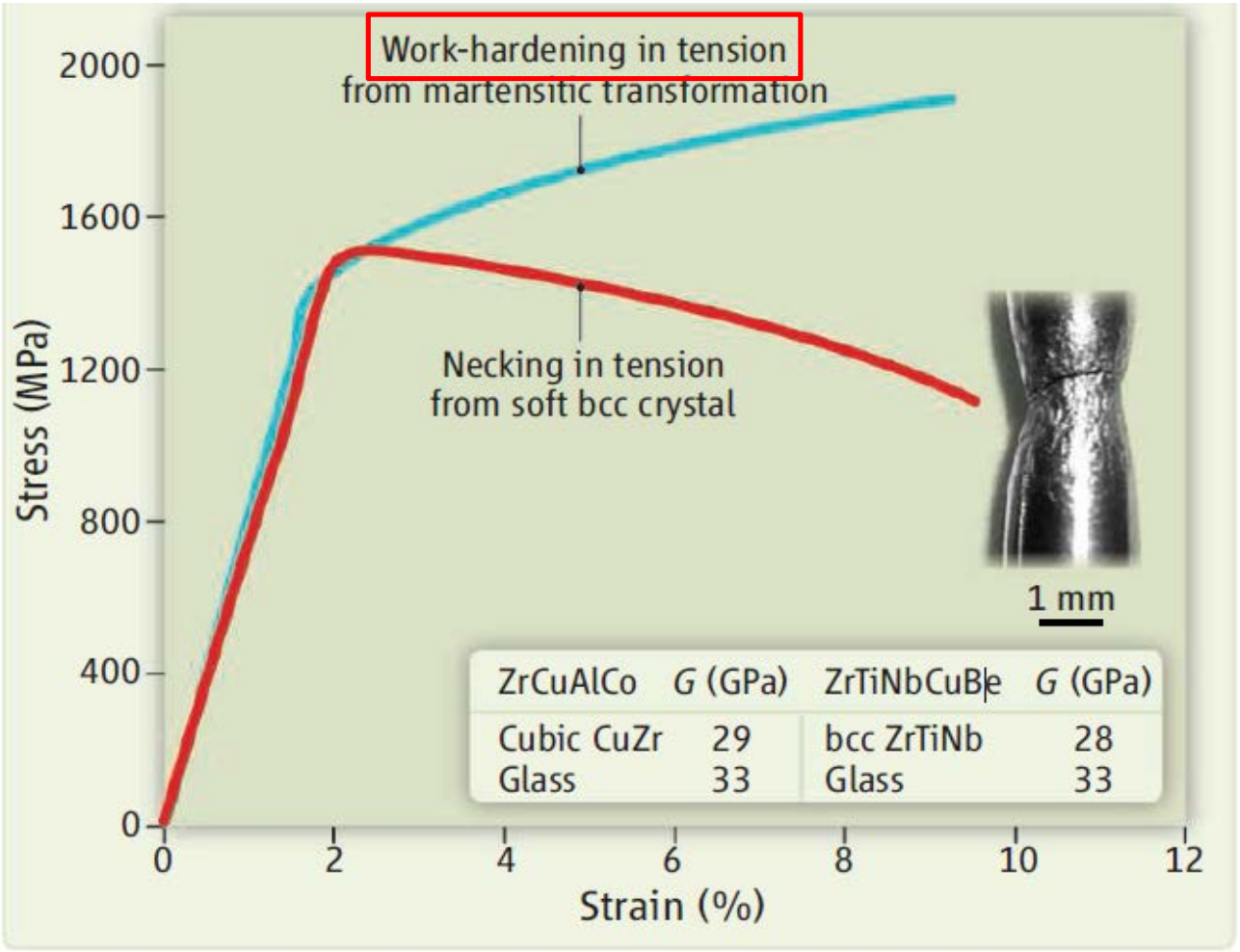

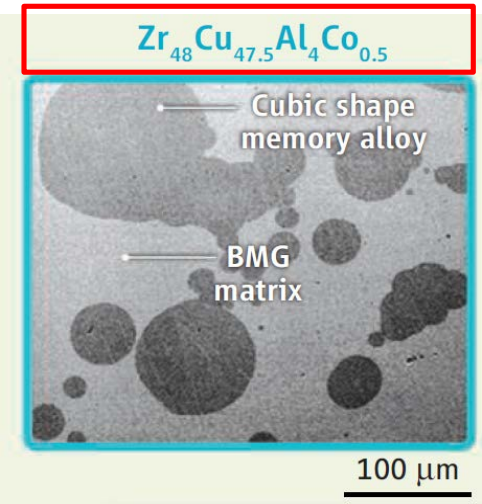

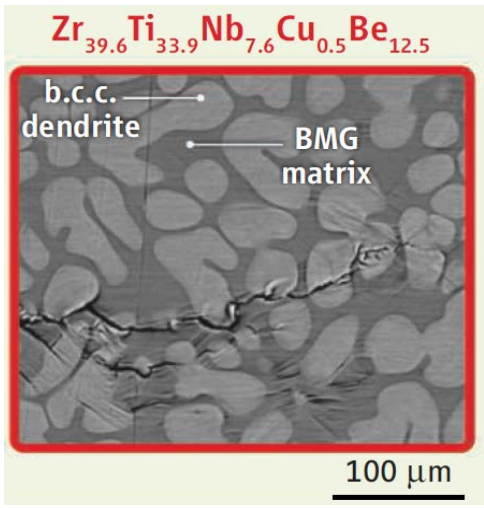

Douglas C. Hofmann, SCIENCE VOL 329 10 SEPTEMBER 2010

2) Work-hardening behavior of BMGCs in tension

Materials Views

www.MaterialsViews.com

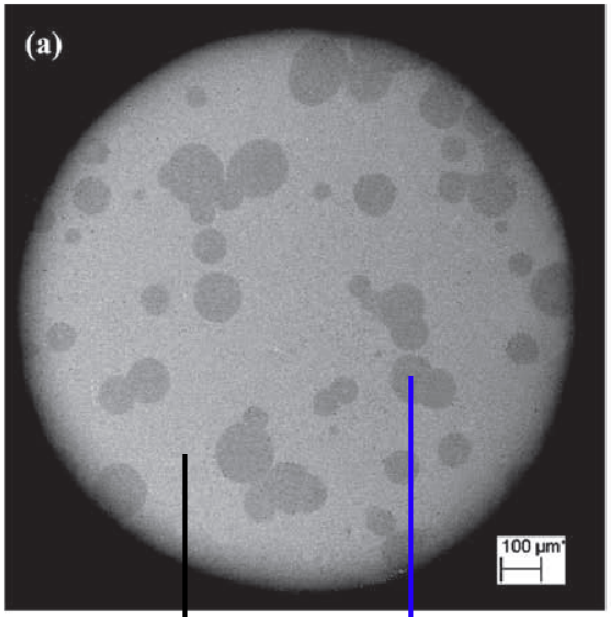

BMG matrix

CuZr B2
Transformation media

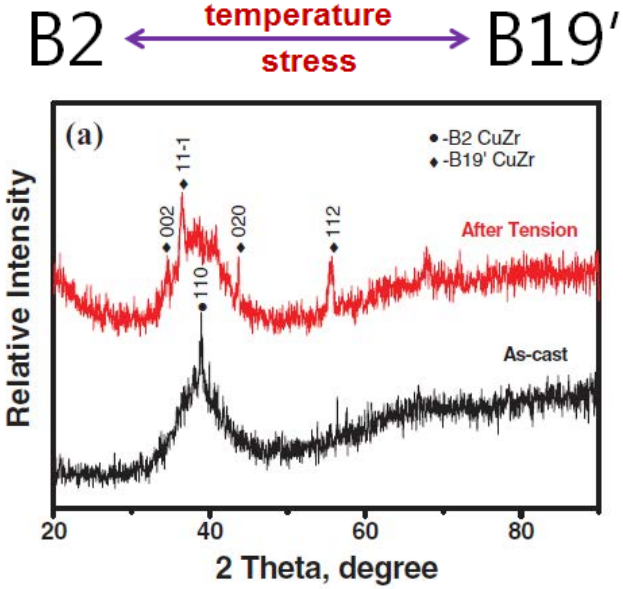

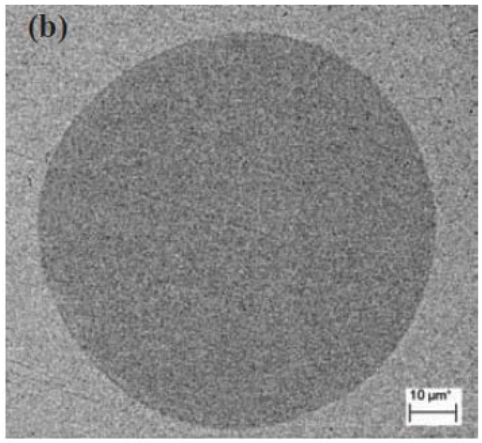

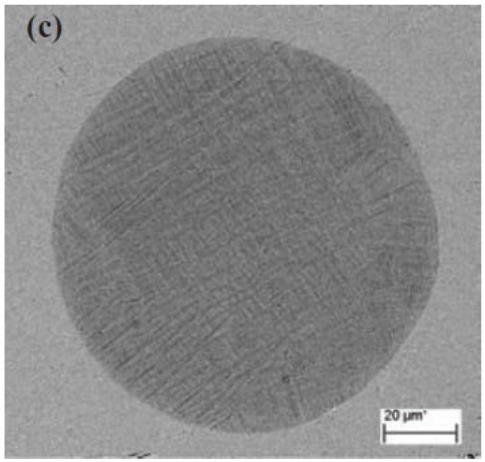

Yuan Wu, et al. Adv. Mater. 2010, 22, 2770–2773

[XRD pattern & Morphology of secondary phase before / after tensile test]

4.7.2 Ex Situ Composites: usually very large volume fraction of second crystalline phase

_ type of reinforcements_pure metals (tungsten, molybdenum, tantalum, nickel, copper and titanium), alloys (1080 steel, stainless steel, and brass), and non-metallics (SiC, diamond, and graphite)

For example: Melt-infiltration technique for the case of long and continuous fibers

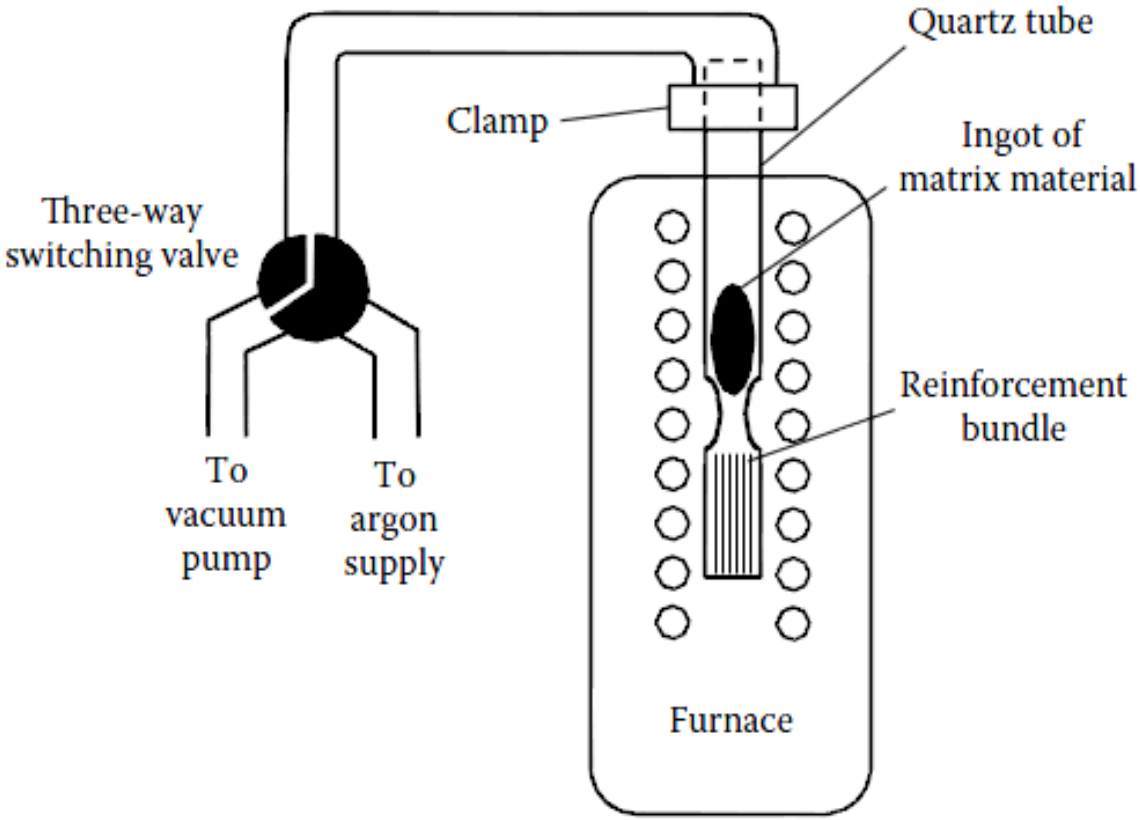

FIGURE 4.14
Schematic of the melt infiltration casting technique to produce *ex situ* BMG composites. (Reprinted from Dandliker, R.B. et al., *J. Mater. Res.*, 13, 2896, 1998. With permission.)

1) Casting : hard/ductile particle

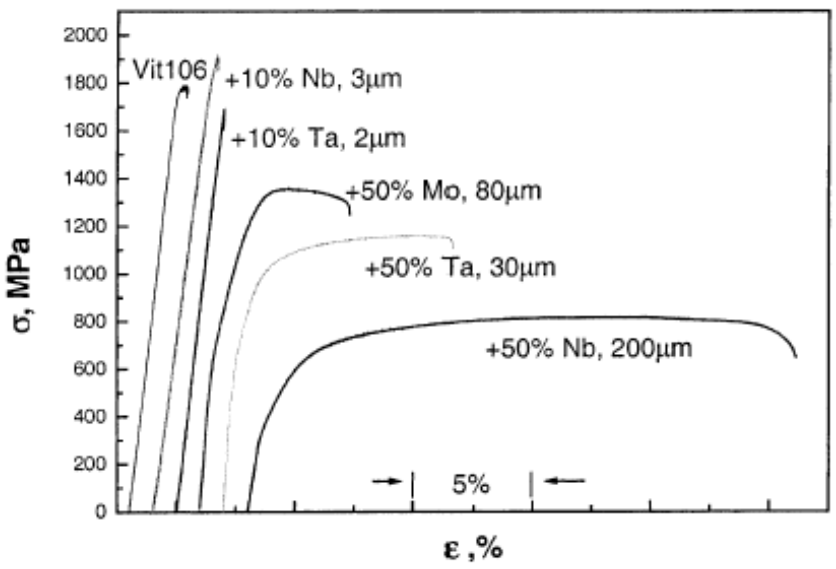

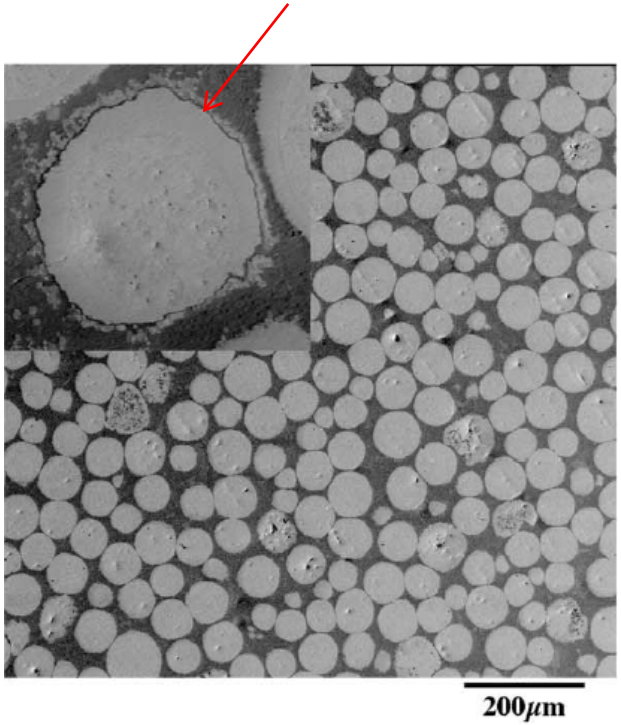

(Johnson et al., Acta Mater.,1999)

2) Extrusion : ductile powder

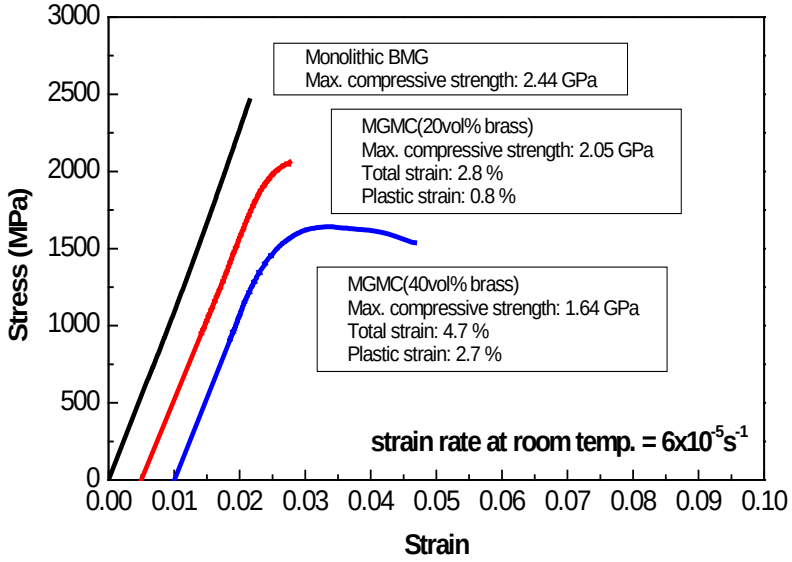

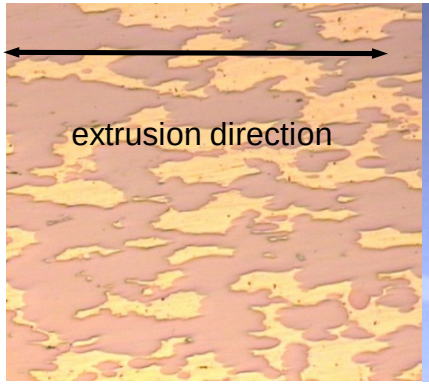

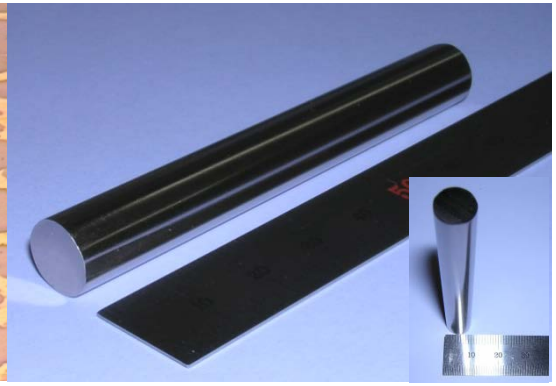

(Kim et al., J. Non-cryst. Solids, 2002)

Compression test: Large plasticity and work-hardening behavior

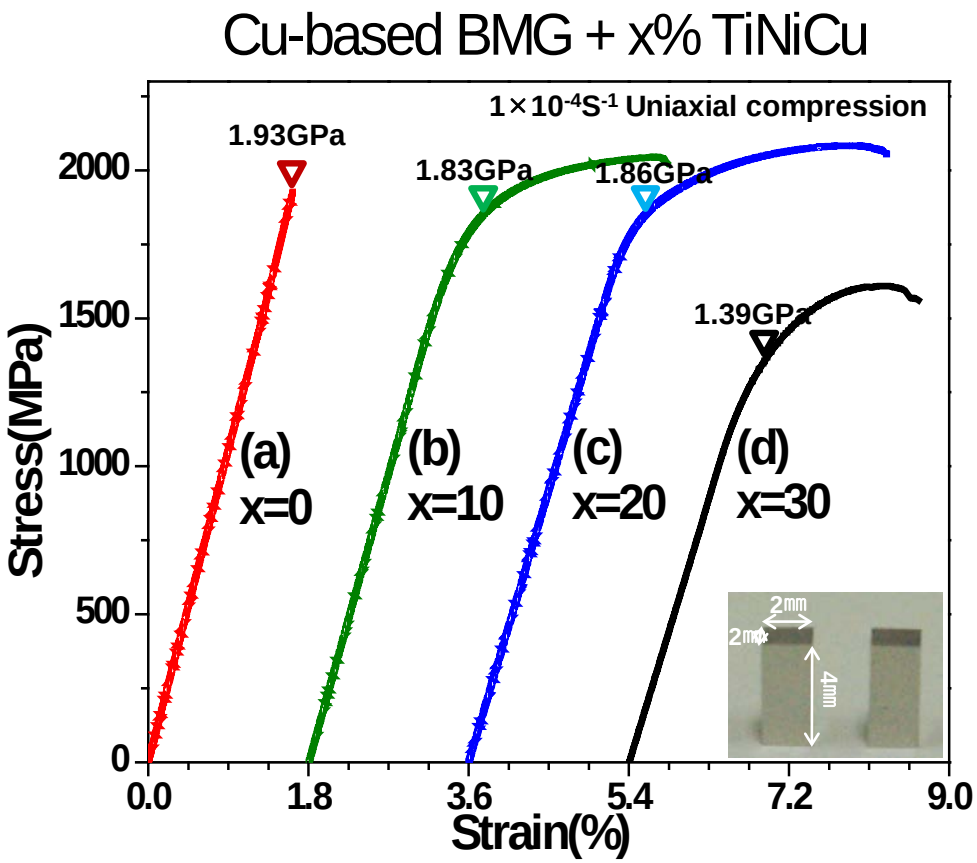

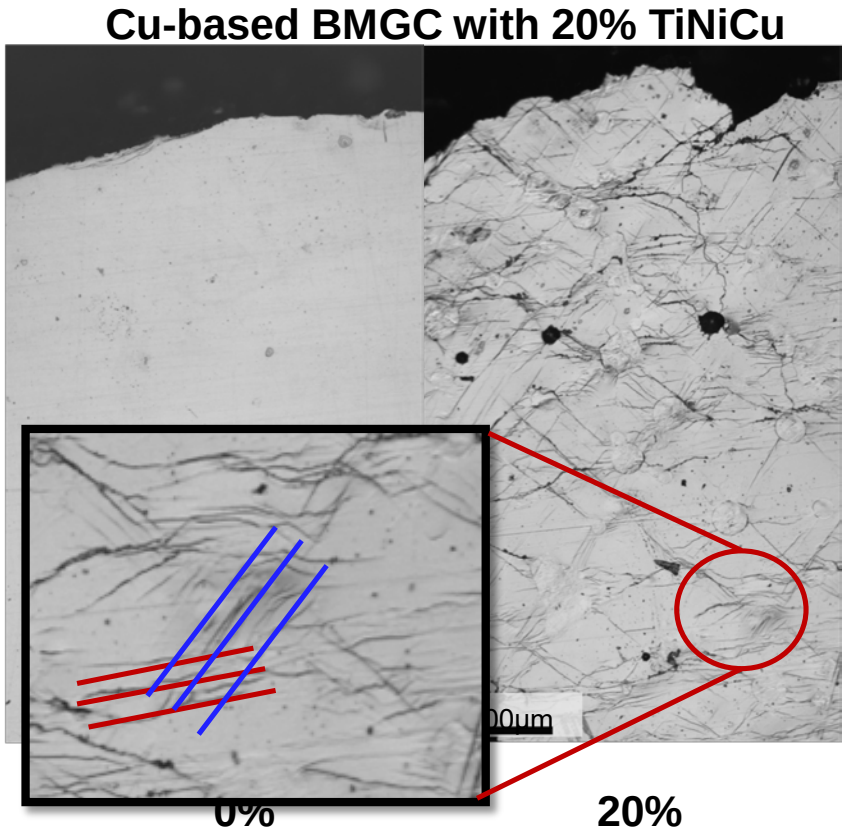

1. Large plasticity and Work hardening behavior
2. Fracture crack – propagate through interface of the 2nd phase and matrix
3. Multiple shear bands: initiation & propagation

Deformation behaviors of BMGC depending on 2nd phase

< Compression >

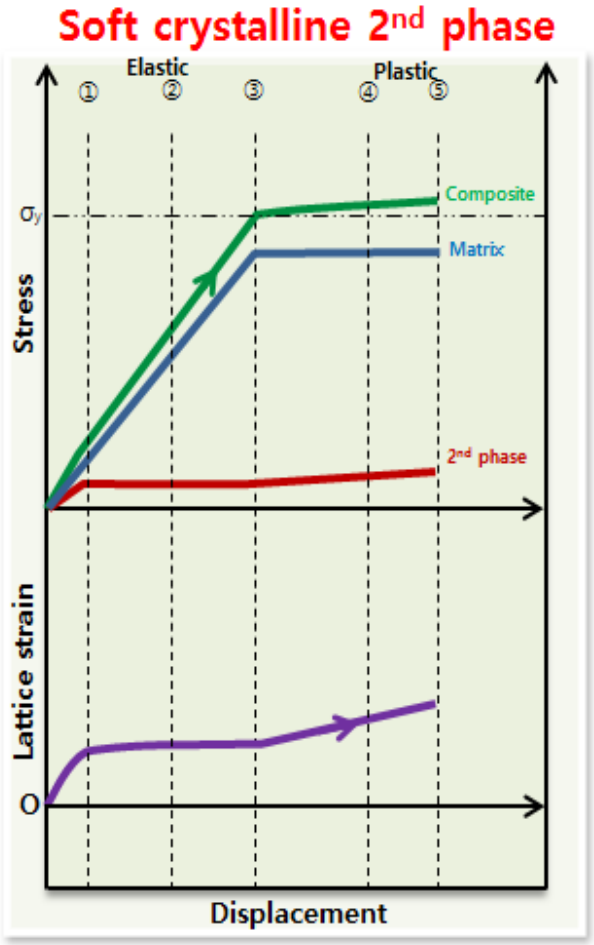

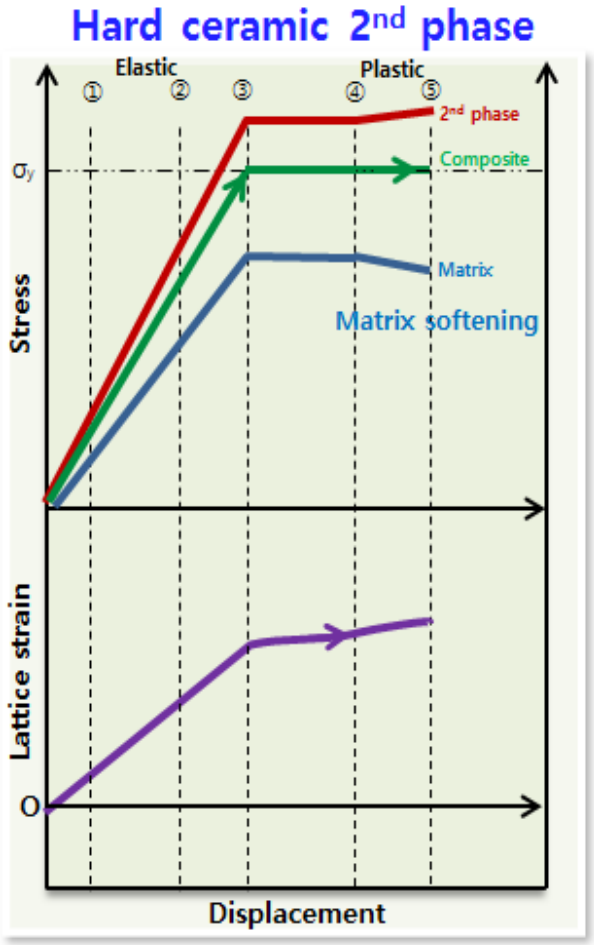

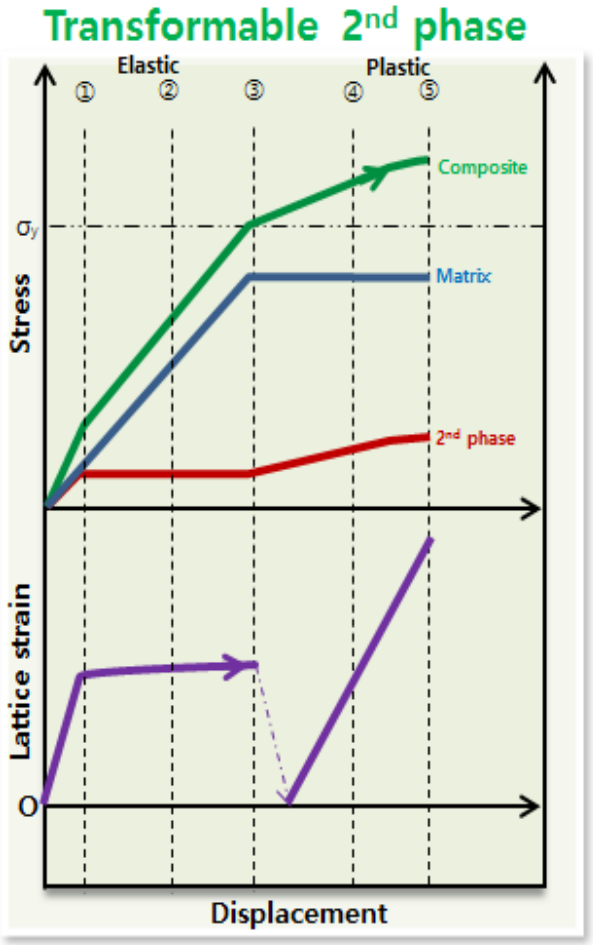

4.9 Bulk Metallic Glass Foams

: have interesting combination of properties such as high stiffness in conjunction with very low specific weight, high gas permeability combined with high thermal conductivity, high mechanical energy absorption, and good acoustic damping.

→ Pores as a gaseous second phase_equally effective in inhibiting catastrophic failures resulting from shear band localization

Pore sizes ranging from the sub-micrometer to the millimeter scale and porosities ranging from 2% to more than 85%

Metallic foams can be classified into closed-cell, partially open-cell, and open-cell types [88]. Closed-cell type metal foams have spatially separated pores and are useful for structural applications such as lightweight construction and energy absorption. On the other hand, open-cell type metal foams have interconnected pores and are useful as functional materials for applications such as electrodes, catalyst support, fluid filters, and biomedical materials. Since the properties of these foams, especially the strength and modulus of elasticity, can be tailored by controlling the volume fraction as well as the structure of pores [91], these materials can be used as biomedical implants. This is because their structure allows bone tissue in-growth leading to the establishment of stable fixation with the surrounding tissues.

Review of the state of the art in the processing of BMG foams I

· $Pd_{43}Cu_{27}Ni_{10}P_{20}$: produced by expansion in the liquid alloy of water vapor bubbles generated from hydrated boron oxide flux powders, followed by quenching.

First porous amorphous metal (2003)
~85 vol%, 200-1000 μm

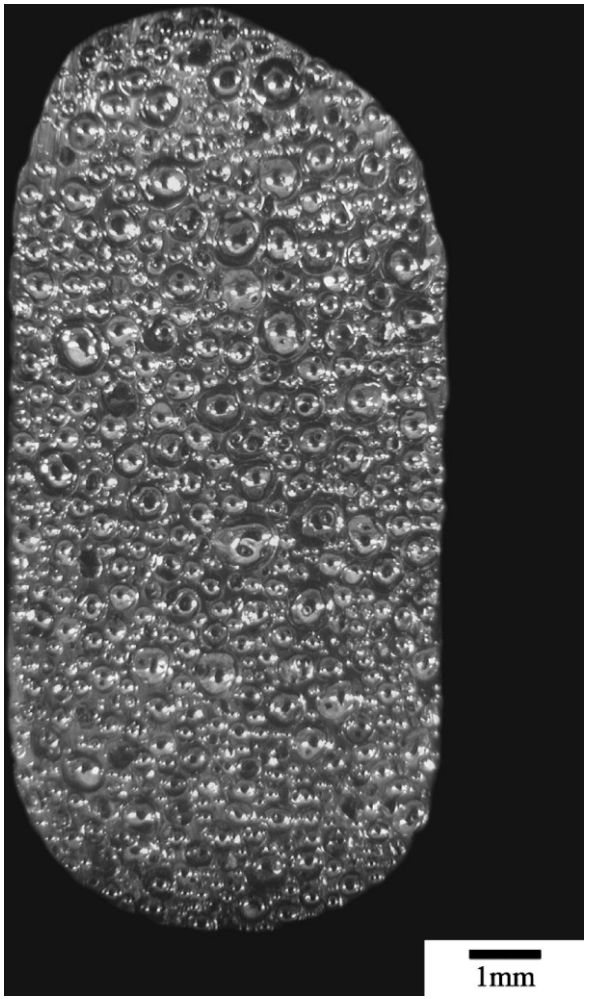

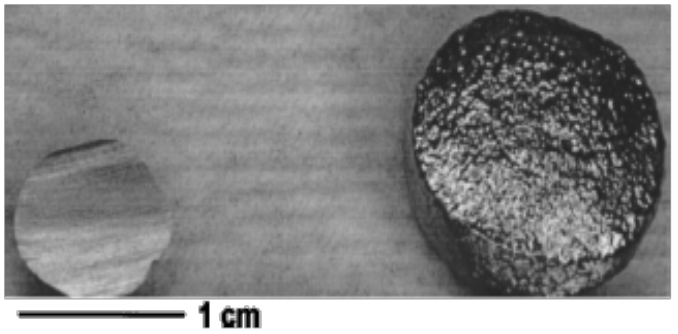

FIG. 11. Size comparison of $Pd_{43}Ni_{10}Cu_{27}P_{20}$ prefoam (left) and expanded foam (right) by rf-coil. The bubble volume fraction of the prefoam is 10%, while that of the final foam is 75%.

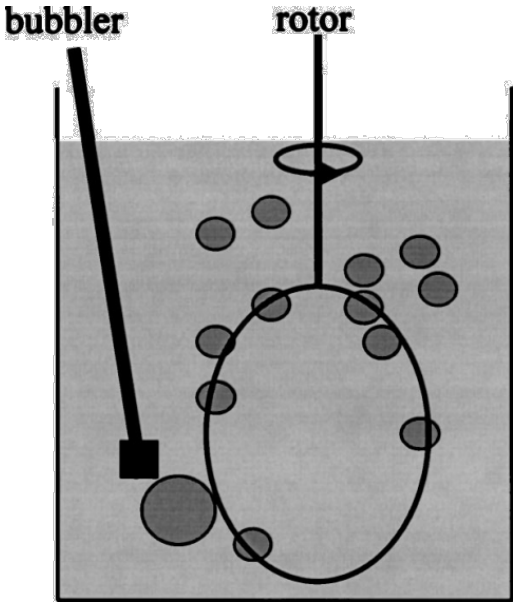

Schematic drawing of the eggbeater constructed for the mechanical air-entrapment method.
The setup comprises a molybdenum brush of 3 cm diameter spinning at speeds of up to 2500 rpm.

Review of the state of the art in the processing of BMG foams II

- **Wada and Inoue → open-cell structures**

(2003) by casting $Pd_{42.5}Cu_{30}Ni_{7.5}P_{20}$ into beds of NaCl particles, quenching, and removing the salt by dissolution.

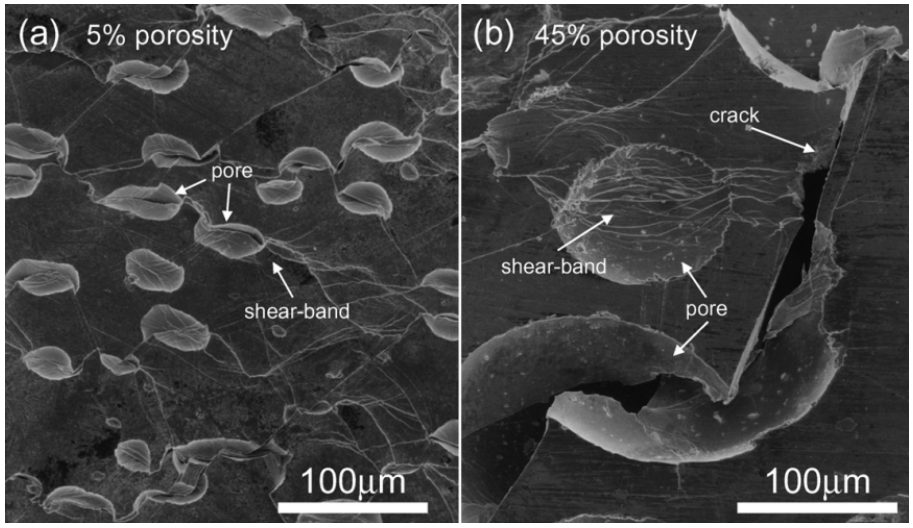

(a and b) SEM images of the surface structure of the porous $Pd_{35}Pt_{15}Cu_{30}P_{20}$ glassy alloy rods with porosities of 5 and 45% deformed up to strains of 0.2 and 0.05, respectively.

~65 vol%, 125-250 μm

(2004) foamed this alloy by the expansion of hydrogen bubbles precipitated from a supersaturated melt.

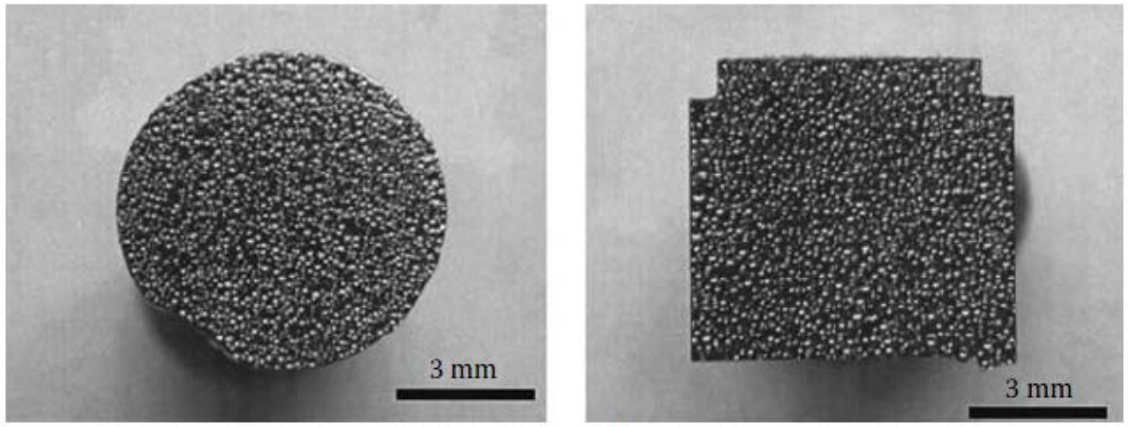

FIGURE 4.16
(a) Transverse cross section and (b) longitudinal cross section of a 7 mm diameter porous $Pd_{42.5}Cu_{30}Ni_{7.5}P_{20}$ alloy rod produced by melting the alloy for 10 min at 813 K under a hydrogen pressure of 1.5 MPa and then water quenching. Note the uniformity of pore size in both the cross sections. (Reprinted from Wada, T. and Inoue, A., *Mater. Trans.*, 45, 2761, 2004. With permission.)

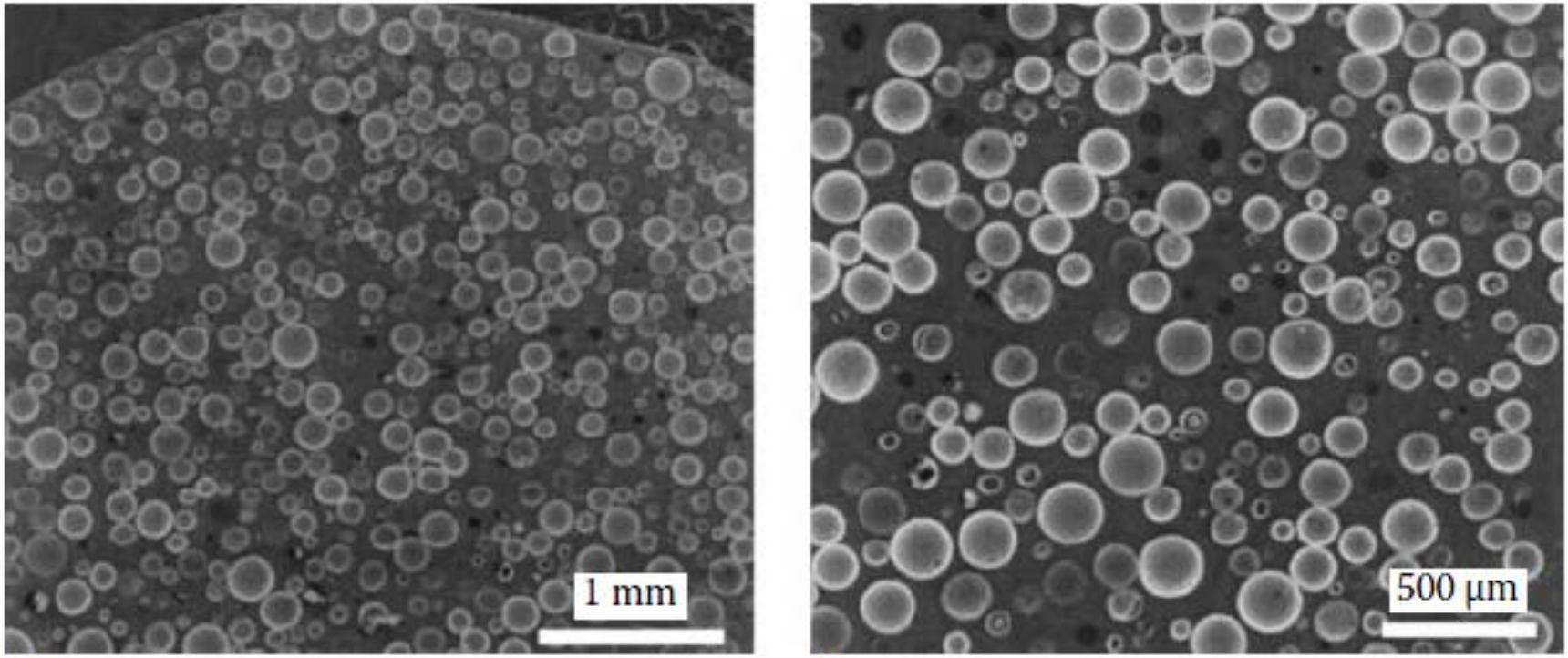

FIGURE 4.17
Scanning electron micrographs of the transverse cross section of the porous glassy $Pd_{42.5}Cu_{30}Ni_{7.5}P_{20}$ alloy rod quenched from 833 K under a hydrogen pressure of 1.5 MPa. The specimen was etched in concentrated H_2SO_4 solution for 3 h to reveal any contrast due to the presence of a crystalline phase. (a) Low-magnification and (b) high-magnification micrographs. Contrast due to the presence of a crystalline phase is not seen even in the high magnification micrograph. (Reprinted from Wada, T. and Inoue, A., *Mater. Trans.*, 45, 2761, 2004. With permission.)

Review of the state of the art in the processing of BMG foams III

- Brothers and Dunand (2004)
  the first amorphous foam using a commercial alloy, $Zr_{57}Nb_5Cu_{15.4}Ni_{12.6}Al_{10}$ (Vit106), which was produced by melt infiltration of beds of hollow carbon microspheres.

- (2005), Brothers et al
  demonstrated the use of the replication method for amorphous foams, in which liquid Vit106 was infiltrated into a packed bed of leachable BaF_2 salt particles that was removed after solidification in an acid bath.

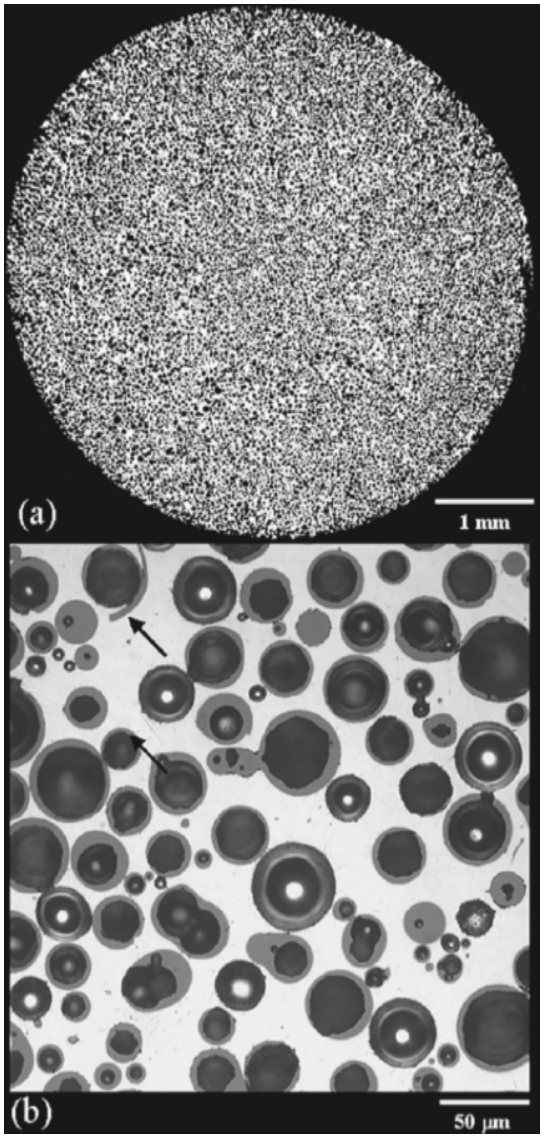

Optical micrographs showing the structure of syntactic Vit106 foam:
a) Low magnification image demonstrating foam uniformity;
b) Magnified image of the surface showing microscopic foam structure. Misshapen carbon microspheres are visible, as is a sphere wall fragment (indicated by Arrow). Good wetting is inferred from the lack of inter-particle porosity.

Review of the state of the art in the processing of BMG foams IV

Two other powder-based methods:

- (2006) Xie et al: reported amorphous $Zr_{55}Cu_{30}Al_{10}Ni_5$ with up to 67% porosity produced by partial spark-plasma consolidation of amorphous powders with diameters of 37–53 mm.

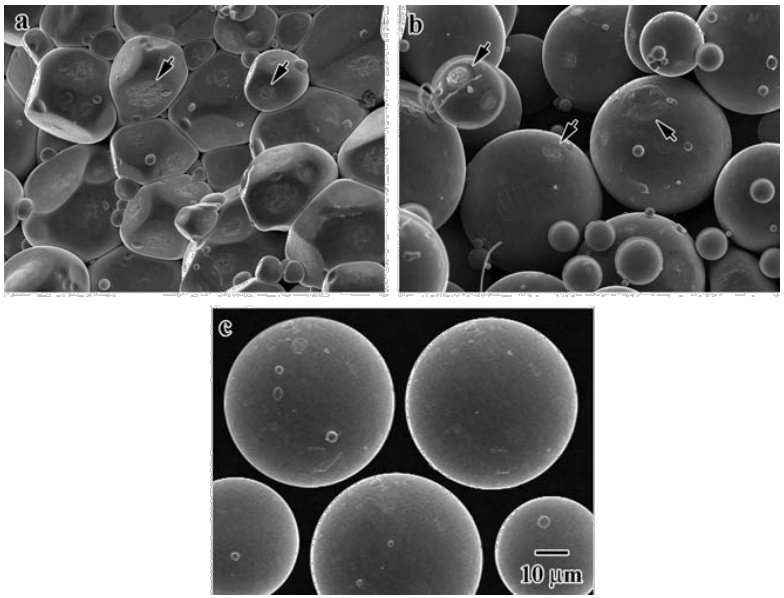

SEM micrographs of the transverse (mechanically crushed) cross section of the sintered porous $Zr_{55}Cu_{30}Al_{10}Ni_5$ bulk glassy alloys with porosities of 4.7% (a), 33.5% (b), and the original powder (c).

- Hasegawa et al studied the effects of lower levels (approximately 2%) of porosity retained in melt-spun ribbons of the same alloy, prepared from powder compacts containing aluminum nitride.

$AlN + Zr\ BMG \rightarrow ZrN + Zr\ BMG + N_2$ bubble

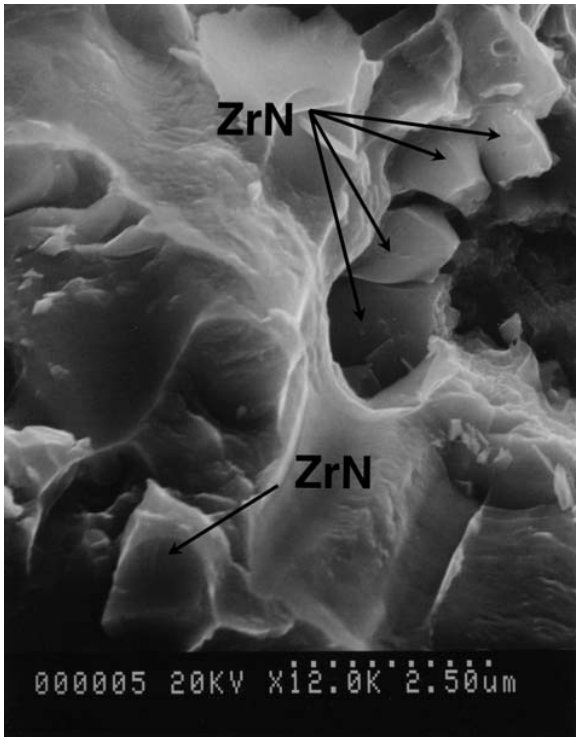

SEM image of the bending fracture surface of a glassy composite alloy ribbon. Synthesized ZrN is indicated by arrows.

Review of the state of the art in the processing of BMG foams V

· (2006), Jayaraj et al
reported successful processing of nanoporous Ti-based amorphous metal ribbons using a method proposed in 2004 by Gebert et al. for a La-based metallic glass, in which one phase is selectively acid-leached from a two-phase amorphous metal.

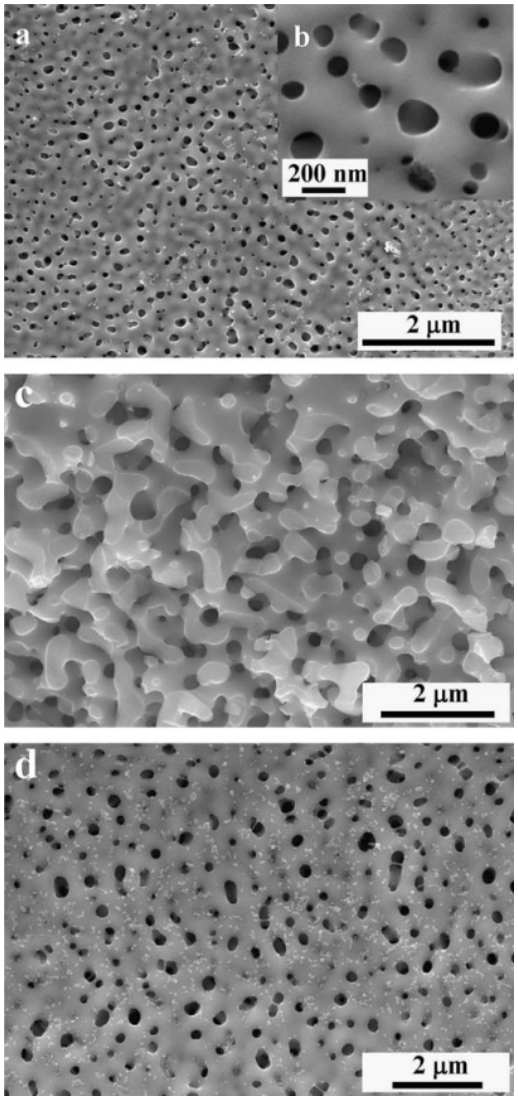

First nano prous amorphous metal
Fully interconnected porosity/ 15-155 nm

SEM images showing the formation of porous morphology of $Y_{20}Ti_{36}Al_{24}Co_{20}$ two-phase amorphous alloy. (a)–(c) Chemically dealloyed $Y_{20}Ti_{36}Al_{24}Co_{20}$ alloy in 0.1 M HNO_3 solution for 24 h:

(a) low magnification demonstrating pore formation;
(b) magnified image showing three-dimensionally connected open type pores;
(c) crosssection of the dealloyed ribbon specimen.
(d) Electrochemically dealloyed $Y_{20}Ti_{36}Al_{24}Co_{20}$ alloy in 0.1M HNO_3 solution with an applied voltage of 1.9 V for 30 min.

Review of the state of the art in the processing of BMG foams VI

· (2006) Lee and Sordelet

where the sacrificial phase is crystalline rather than amorphous, and the starting two phase material is formed by warm extrusion of powder blends rather than casting.

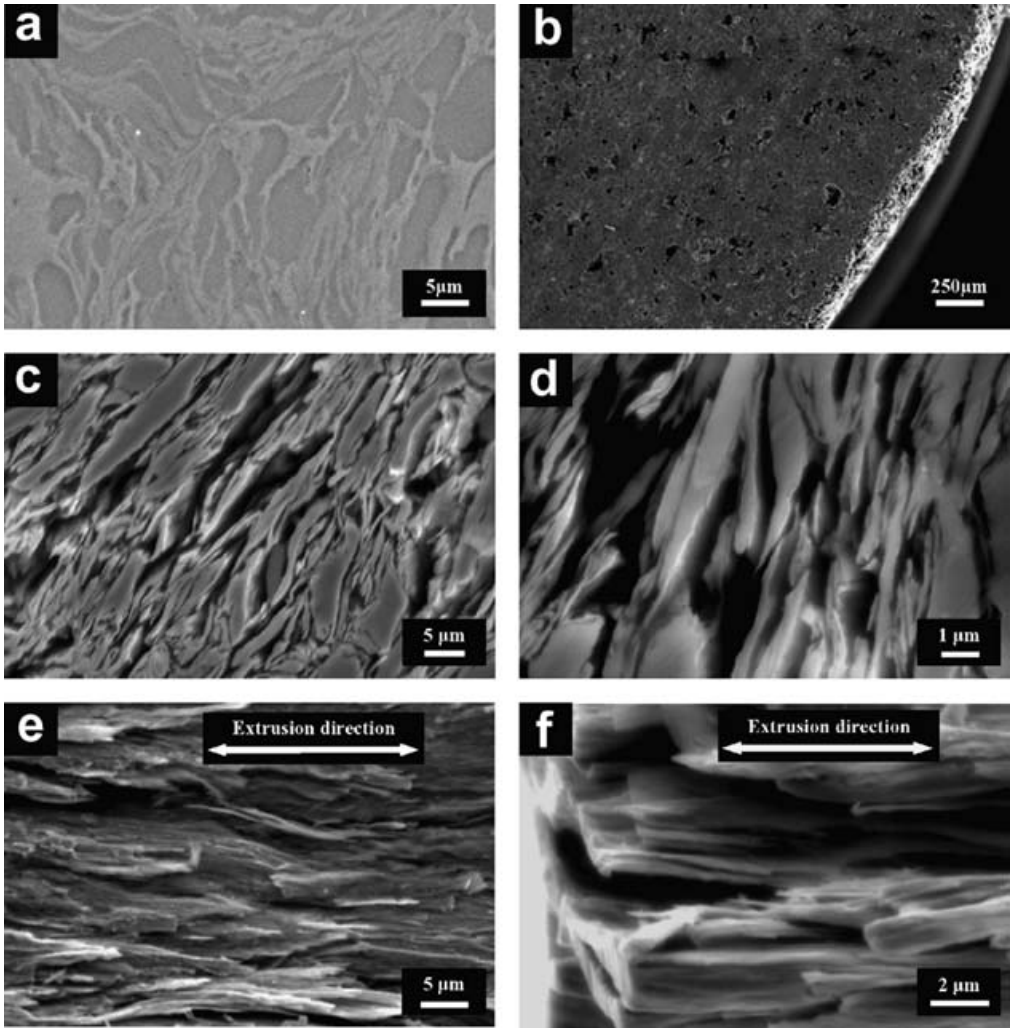

SEM images of porous $Cu_{47}Ti_{33}Zr_{11}Ni_8Si_1$ MG. Pores are uniformly distributed throughout the sample.

(a) Transverse polished cross section of $Cu_{47}Ti_{33}Zr_{11}Ni_8Si_1$ MG + Cu composite precursor before dissolution of the Cu;
(b) macrostructure of porous $Cu_{47}Ti_{33}Zr_{11}Ni_8Si_1$ MG;
(c) transverse cross-sectional microstructure of porous $Cu_{47}Ti_{33}Zr_{11}Ni_8Si_1$ MG;
(d) enlarged image of (c);
(e) longitudinal microstructure of porous $Cu_{47}Ti_{33}Zr_{11}Ni_8Si_1$ MG;
(f) detailed microstructure obtained from the lateral surface of the porous $Cu_{47}Ti_{33}Zr_{11}Ni_8Si_1$ MG.

Images of several representative porous amorphous metals, produced using liquid-state methods, are shown in Figure 1.
These methods demonstrated the possibility of foaming reactive Zr-based alloys of the sort used in most metallic glass applications.

Representative powder-processed porous amorphous metals are shown in Figure 2.

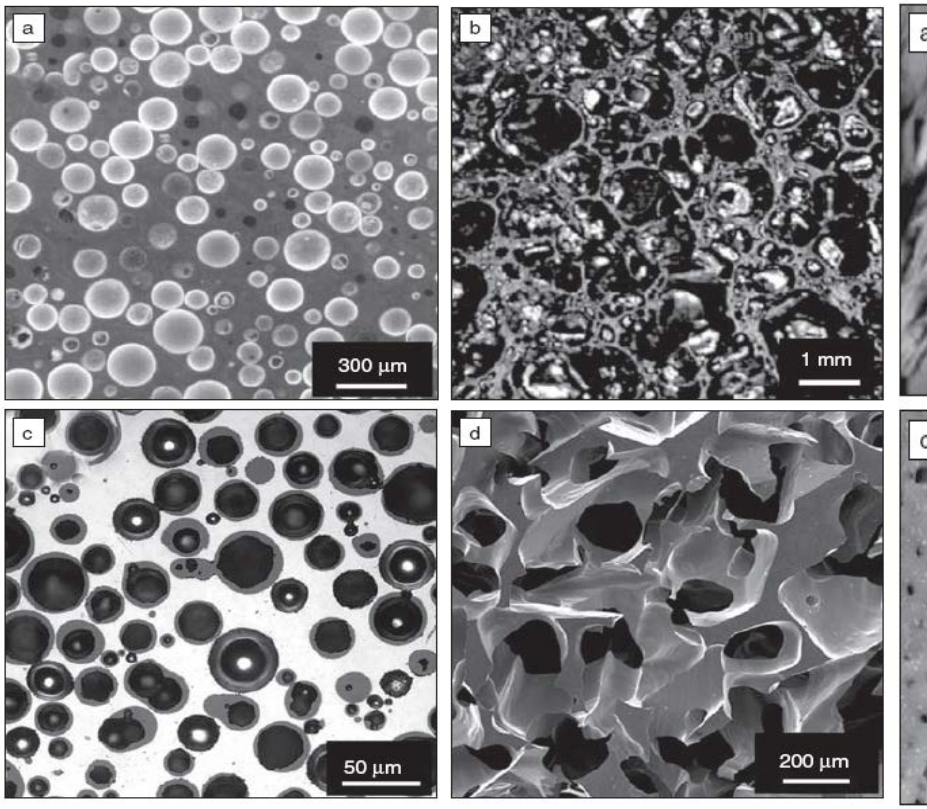

Figure 1. Examples of amorphous metal foams created by liquid-state and supercooled-liquid-state methods. (a) Pd-based foam (porosity $P = 42–46\%$) made by precipitation of dissolved hydrogen gas during cooling.[7] (b) Pd-based foam ($P = 85\%$) made by entrapping gas in the melt and then expanding it in the supercooled-liquid state.[5] (c) Zr-based foam made by infiltration of a bed of hollow carbon spheres. Volume fraction of spheres in the foam is 59%.[12] (d) Zr-based foam ($P = 78\%$) made by infiltration of BaF_2 salt particles followed by removal of those particles in an acid bath.[14]

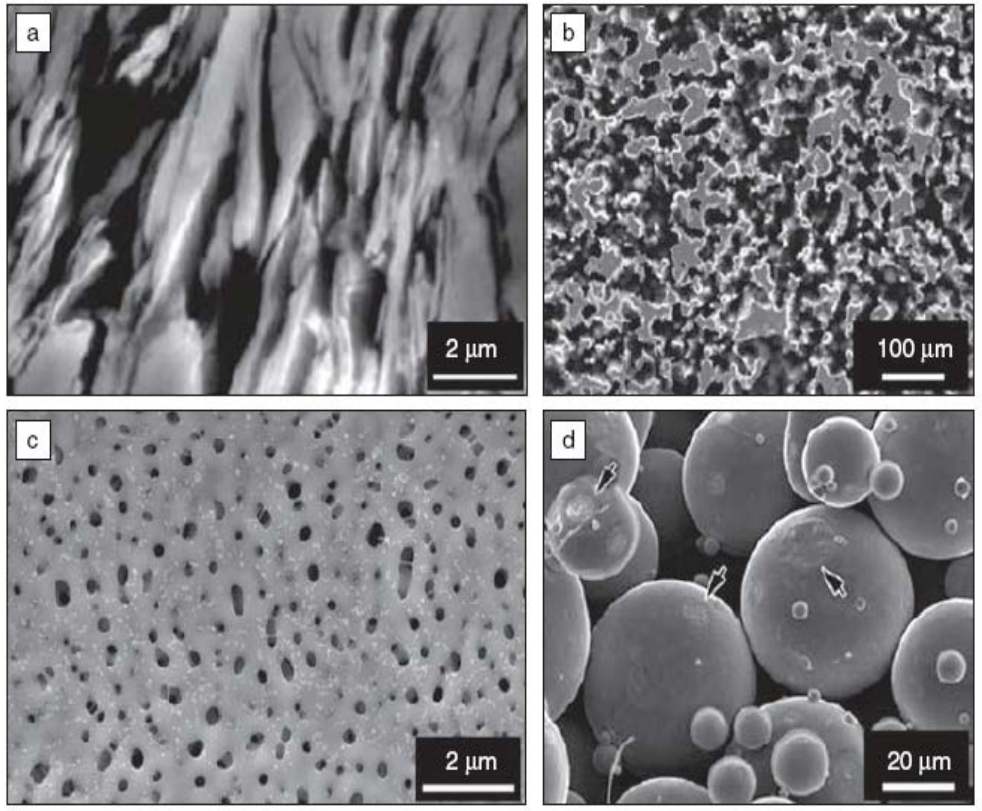

Figure 2. Examples of powder-processed porous amorphous metals and amorphous metal foams created by solid-state methods. (a) Cu-based foam (porosity $P = 75\%$) made by dissolution of crystalline Cu from an extruded composite.[21] (b) Ni-based foam ($P = 42\%$) made by dissolution of brass from an extruded composite.[22] (c) Ti-based porous amorphous metal (P not given) made by selective dissolution of one phase from a two-phase amorphous metal.[19] (d) Zr-based porous compact ($P = 34\%$) made by partial electroconsolidation of amorphous powders.[23]

Mechanical Properties (1)

The primary purpose of introducing porosity in amorphous metals is to hinder the propagation of shear bands.

Two main mechanisms of hindering shear-band propagation have been identified : shear-band disruption and shear-band stabilization.

i) shear-band disruption

→ (the same mechanisms active in amorphous metal-matrix composites) : Pores (like solid inclusions) interrupt shear bands when their paths intersect, favoring branching of those bands and/or nucleation of new bands.

ii) shear-band stabilization

→ (first noted during bending of thin amor. metal wires and foils)

a) each band relaxes the stress from a smaller volume of the surrounding glass, enabling a closer spacing of the neighboring shear bands subsequently initiated, thereby increasing band density and overall plastic strain.
b) shallower shear bands produce smaller shear offsets at the surfaces of the wires or foils, and these smaller offsets reduce the probability of nucleating a crack. In the case of Zr-based alloys, shear-band stabilization becomes noticeable for wire or foil thicknesses below about 1 mm.

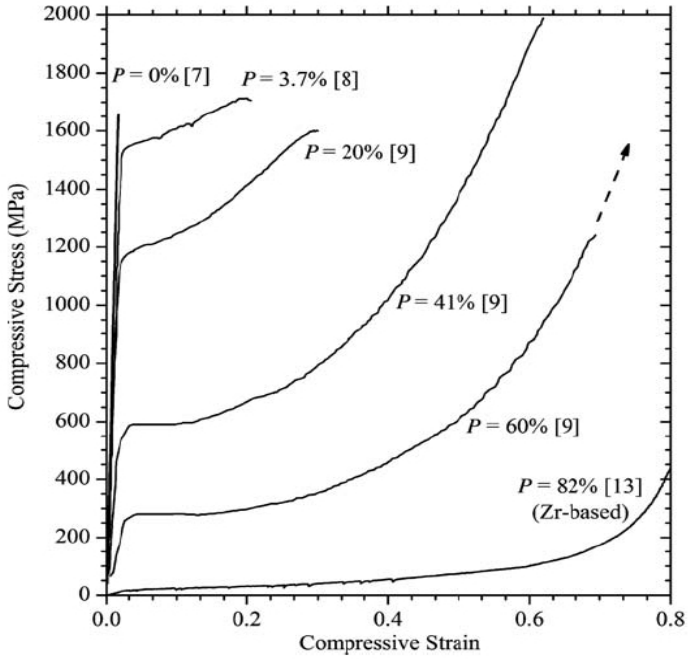

Figure 3. Compressive engineering stress–strain curves for several porous amorphous metals at intervals of approximately 20% porosity *P*. All but the highest-porosity material (which was processed from $Zr_{57}Nb_5Cu_{15.4}Ni_{12.6}Al_{10}$) were processed from $Pd_{42.5}Cu_{30}Ni_{7.5}P_{20}$.

The effectiveness of porosity in improving ductility and energy absorption in amor. metals, several compressive stress–strain curves for porous amorphous metals with porosities between **3.7% and 82%** are shown in Figure

→ With increased porosity, the amorphous samples show decreasing strength and stiffness

Mechanical Properties(2)

A more comprehensive illustration of compressive ductility in porous amorphous metals is shown in Figure where failure strains are compiled as a function of porosity.

→ pore morphology & the effectiveness that determine the effectiveness of the ductilizing mechanisms_ some structures lead to almost no ductilization even at relatively high porosity.

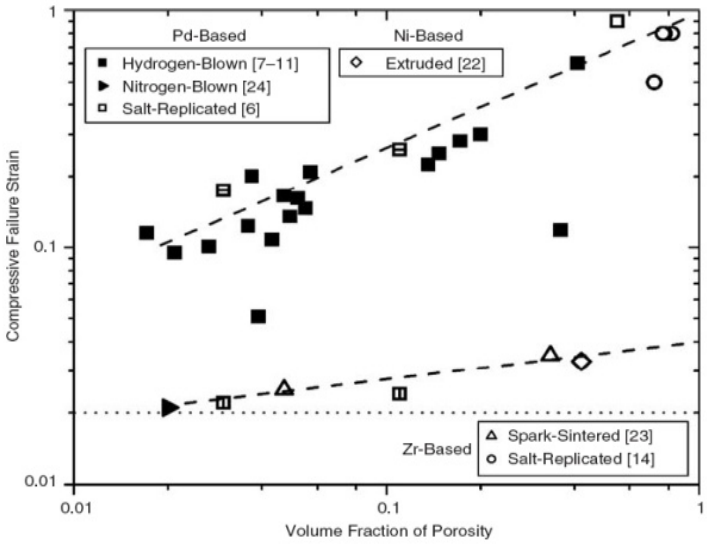

Figure 4. Compressive strain to failure as a function of porosity for published porous amorphous metals. Composition and processing methods are summarized in the labels. Open and solid symbols represent open-cell and closed-cell structures, respectively. Open squares with strikethroughs represent materials with elliptical porosity oriented parallel (vertical strikethroughs) and perpendicular (horizontal strikethroughs) to the loading axis.[9] The horizontal line at a failure strain of 2% is representative of fully dense amorphous metals.[1] The dashed lines are visual aids used to demonstrate how certain structures (upper line) produce substantial ductility, while others (lower line) produce less ductility.

Available data for the compressive yield strength and loading stiffness of porous amorphous metals are compiled in Figure

porous amorphous metals span a wide range of strengths, from less than 10 MPa for high-porosity foams to nearly 2 GPa for near-dense alloys.

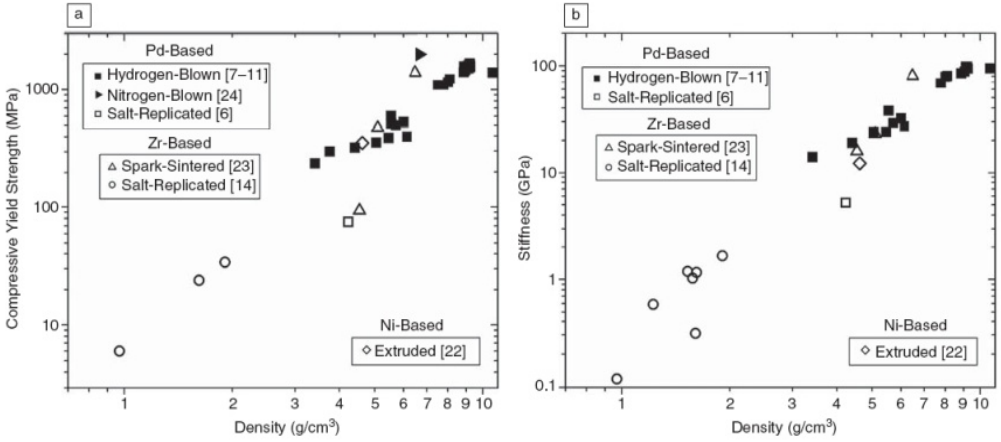

Figure 5. (a), (b) Compressive yield strength and stiffness as functions of density for published porous amorphous metals. Composition and processing methods are summarized in the labels. Open and solid symbols represent open-cell and closed-cell structures, respectively. Densities of the pore-free Zr-, Ni- and Pd-based glasses are 6.8 g/cm³, 7.9 g/cm³, and 9.4 g/cm³, respectively.

Applications

- Porosity can be used as a means of selectively and continuously trading strength and stiffness for ductility, weight reduction, and energy absorption

⟷

- Porous amorphous metals could find use in a variety of applications, from structural materials to energy absorption or packaging applications

High strength & compressive application
→ only small relative losses in strength

At larger porosities, better energy absorption capacity, when compared on a volumetric basis, than crystalline Al-based foams

· The intrinsic benefits of AM
→Large elastic energy return, wear resistance, and corrosion resistance and so on.

· Limitation
→ Low tensile ductility, cooling rate, high costs

· Unknown
→ Resistance to fatigue and tensile fracture

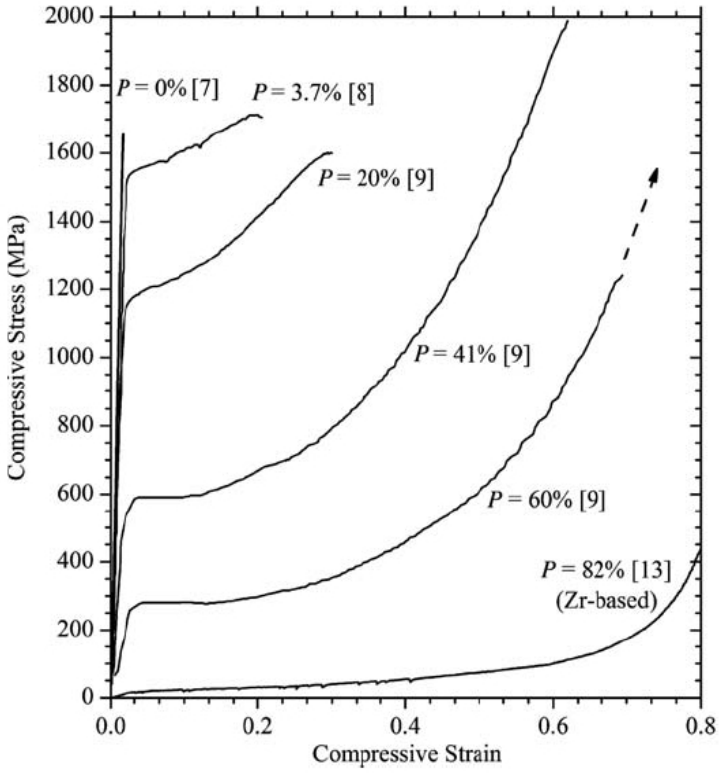

Figure 3. Compressive engineering stress–strain curves for several porous amorphous metals at intervals of approximately 20% porosity *P*. All but the highest-porosity material (which was processed from $Zr_{57}Nb_5Cu_{15.4}Ni_{12.6}Al_{10}$) were processed from $Pd_{42.5}Cu_{30}Ni_{7.5}P_{20}$.

Summary of BMG foam

Porous amorphous metals represent a promising new step toward the engineering application of amorphous metals by enabling mechanical properties and density to be varied across a wider range than is possible using monolithic alloys or composites.

- compressive failure strains
  → can be varied from near-maximum values

- compressive strength and stiffness
  → can be varied from ~2% to more than 80%

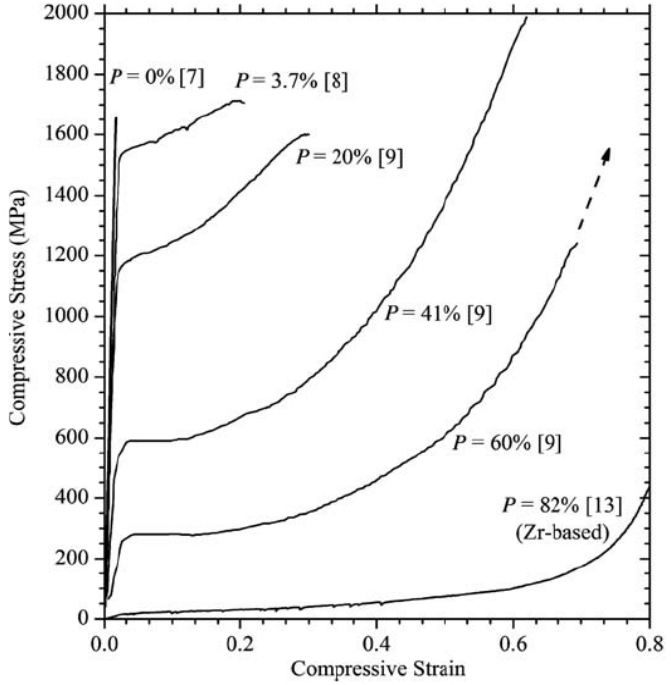

Figure 3. Compressive engineering stress–strain curves for several porous amorphous metals at intervals of approximately 20% porosity *P*. All but the highest-porosity material (which was processed from $Zr_{57}Nb_5Cu_{15.4}Ni_{12.6}Al_{10}$) were processed from $Pd_{42.5}Cu_{30}Ni_{7.5}P_{20}$.

Porosity introduction can optimize density-compensated mechanical properties and tailor other properties such as fluid permeability, specific surface area, and acoustic damping.

5 Crystallization Behavior

Crystallization in TTT diagram.

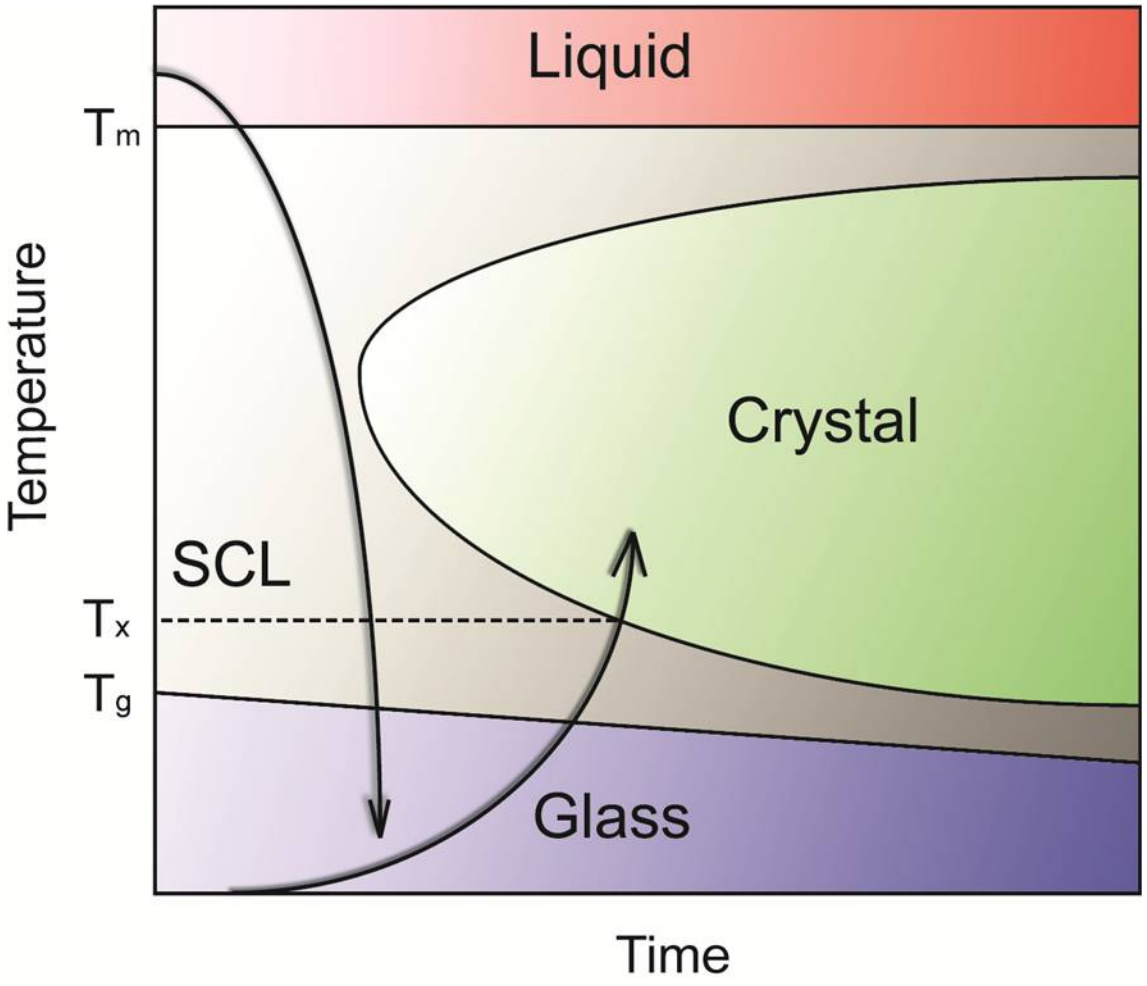

Glass Formation

Retention of liquid phase

⇕

Formation of
Crystalline phase

Cooling Process.

Crystal vs. Glass

→ Thermodynamics

Kinetics

5 *Crystallization Behavior*

Crystallization to Equilibrium or Non-equilibrium Phase.

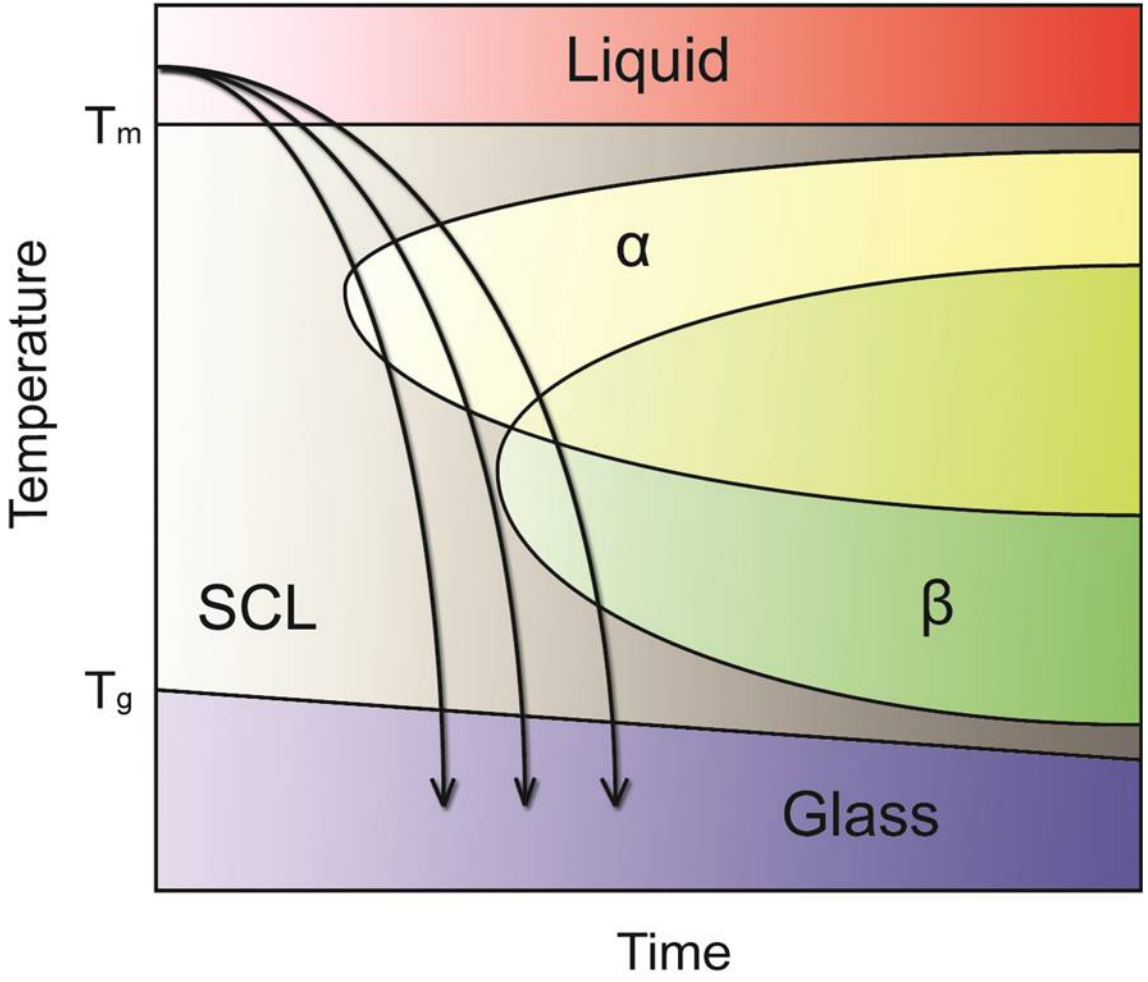

α : Equilibrium phase

β : Non-Equilibrium phase

Cooling Process.

Only α phase

Heating Process.

Low T Crystallize to β

High T Crystallize to α

5 Crystallization Behavior

Annealing Method.

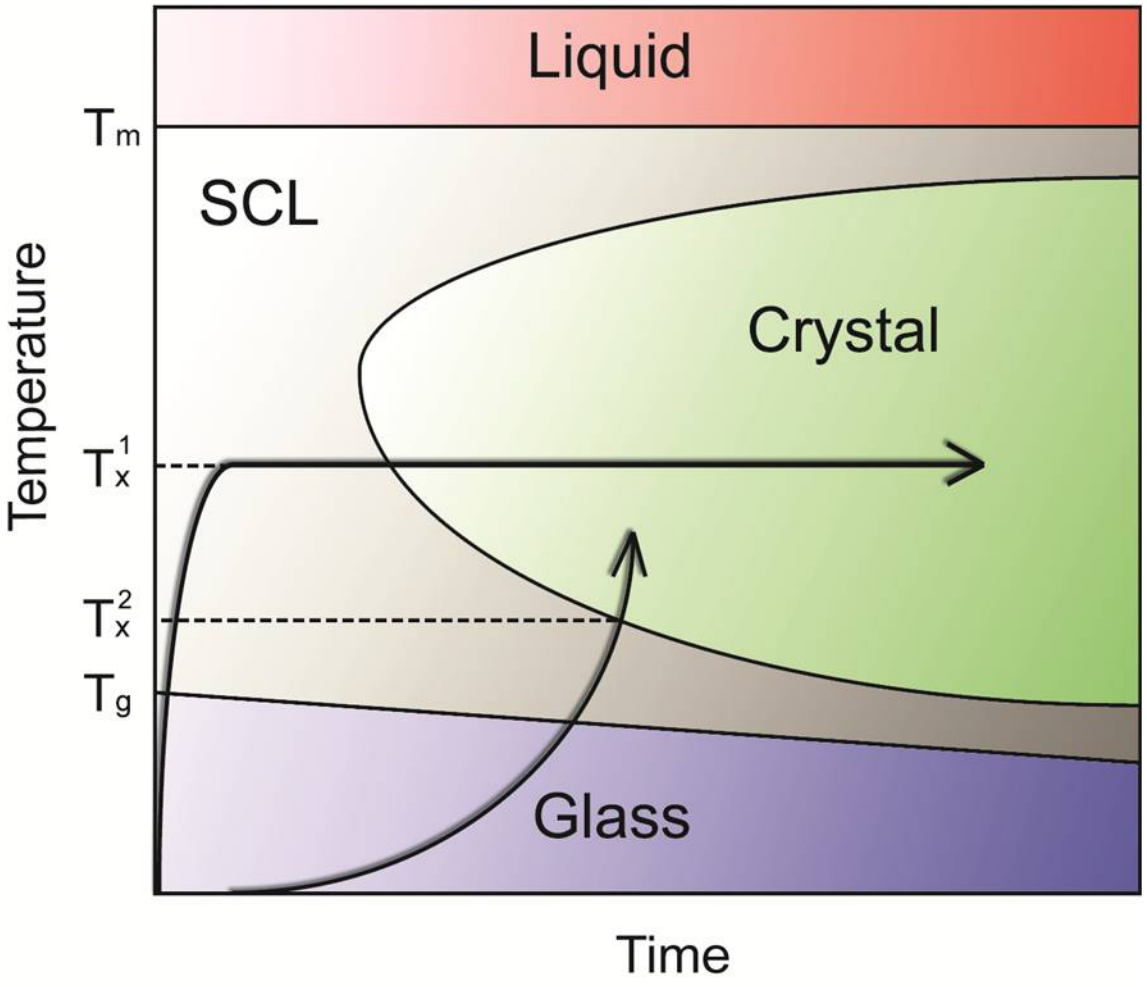

Heating Process.

Glass ➡ *Crystal*

1. Isothermal Heating
2. Continuous Heating

(Annealing temperature has to be higher than T_g)

⬇

Crystallization

5 Crystallization Behavior

Crystallization to Equilibrium or Non-equilibrium Phase.

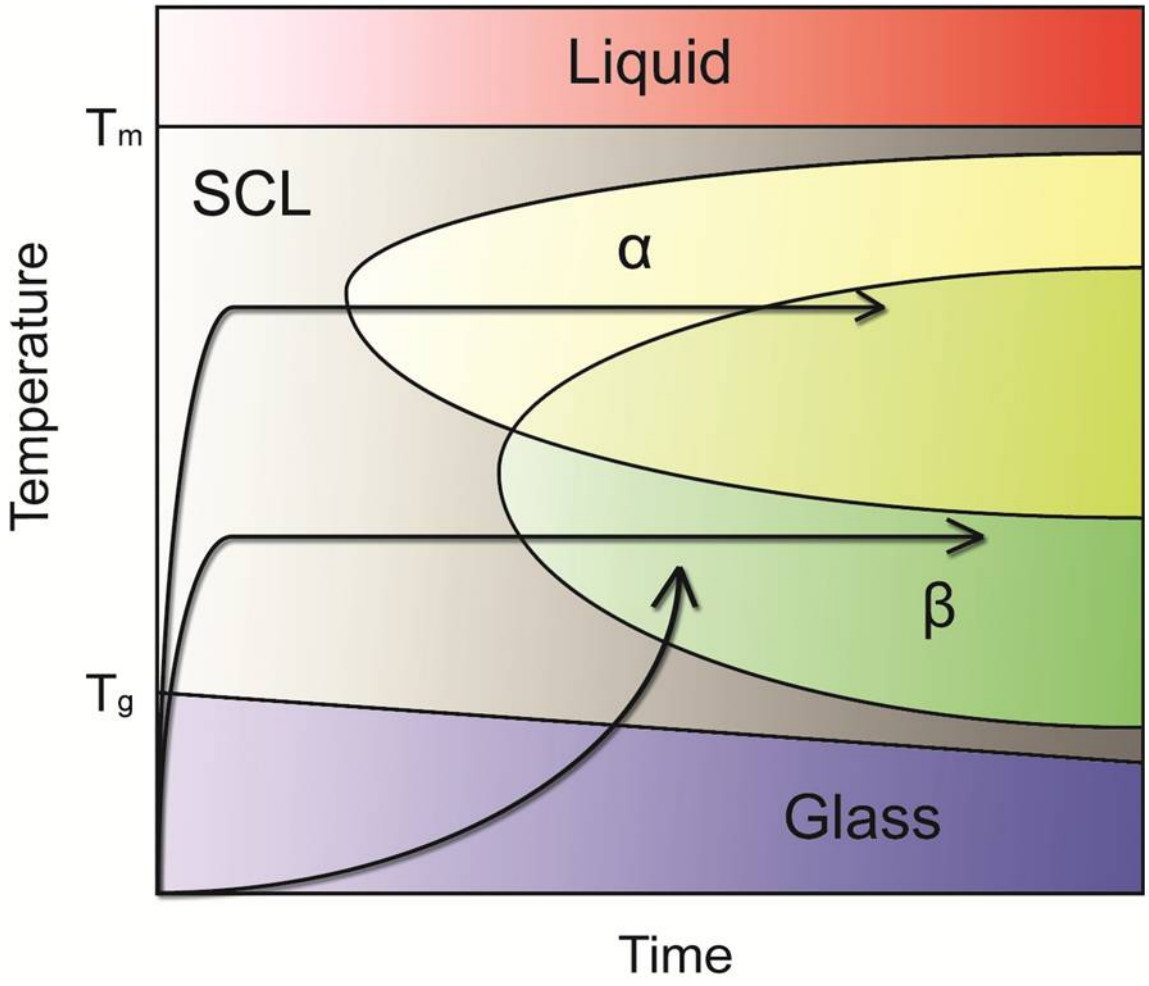

α : Equilibrium phase

β : Non-Equilibrium phase

Cooling Process.

Only α phase

Heating Process.

Low T Crystallize to β

High T Crystallize to α

5 *Crystallization Behavior*

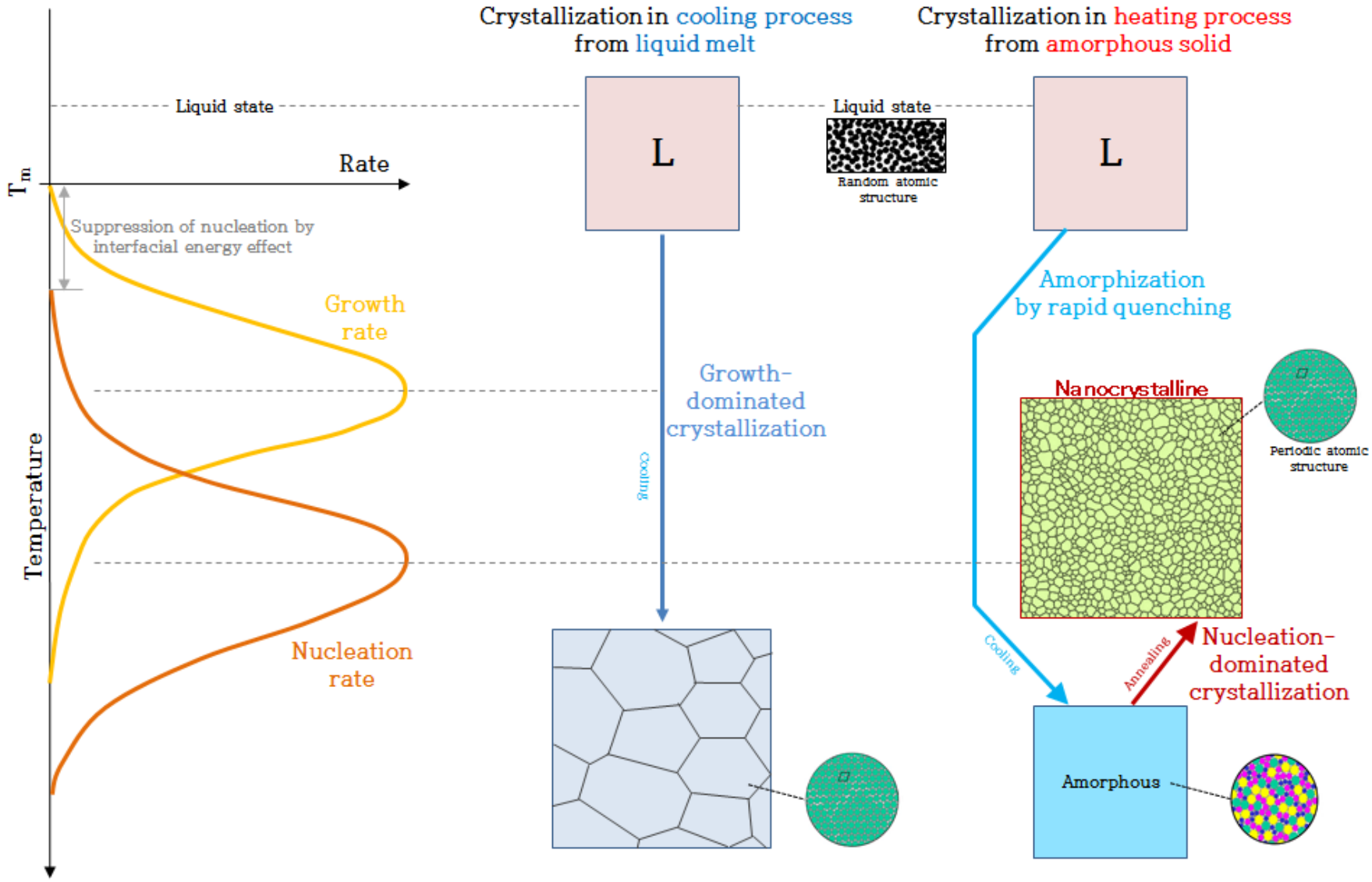

5

Crystallization Behavior

Temp. or Pressure ↓

Amorphous phase → crystal phase

(high E (metastable) state)

Tailor the microstructure to obtain a glass+nanocrystal or an ultrafine-grained composite, or a completely crystalline materials of different grain sizes by controlling the time and temperature of crystallization.

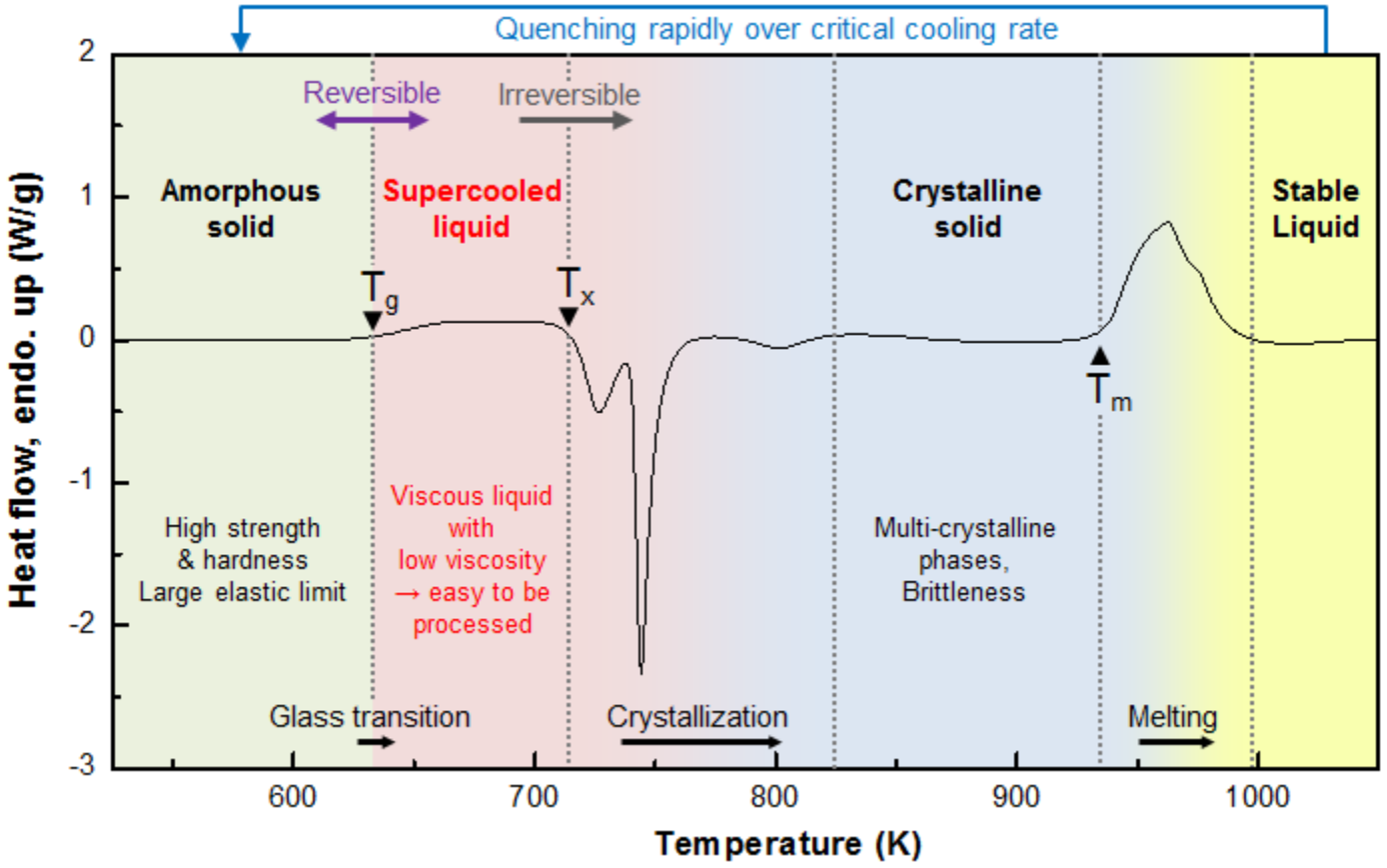

DSC trace of Vitreloy 1 substrate and the temperature regions sectioned according to phase transformations

5

Crystallization Behavior

Temp. or Pressure ↓

Amorphous phase → crystal phase

(high E (metastable) state)

Tailor the microstructure to obtain a glass+nanocrystal or an ultrafine-grained composite, or a completely crystalline materials of different grain sizes by controlling the time and temperature of crystallization.

1) Importance for scientific point of view

: Crystallization of metallic glasses occurs by a nucleation and growth process, it offers an opportunity to study the growth of crystals into an isotropic medium. Further, this process also offers a chance to test the classical nucleation and growth theories at large undercooling.

2) Importance for technological point of view

: ① The crystallization temperature of metallic glasses provides a real upper limit to the safe use of metallic glasses without losing their interesting combination of properties. The important and interesting properties of metallic glasses are lost as a result of crystallization.

② Metallic glass ribbons were found to lose their bend ductility upon crystallization. But, it should be realized that Tx cannot be taken as an indicator of the safe operating temperature of a metallic glass. For example, even though many Fe-based metallic glasses have Tx in the region of 400℃, their maximum long-term operating temperatures are only of the order of 150℃.

5 *Crystallization Behavior*

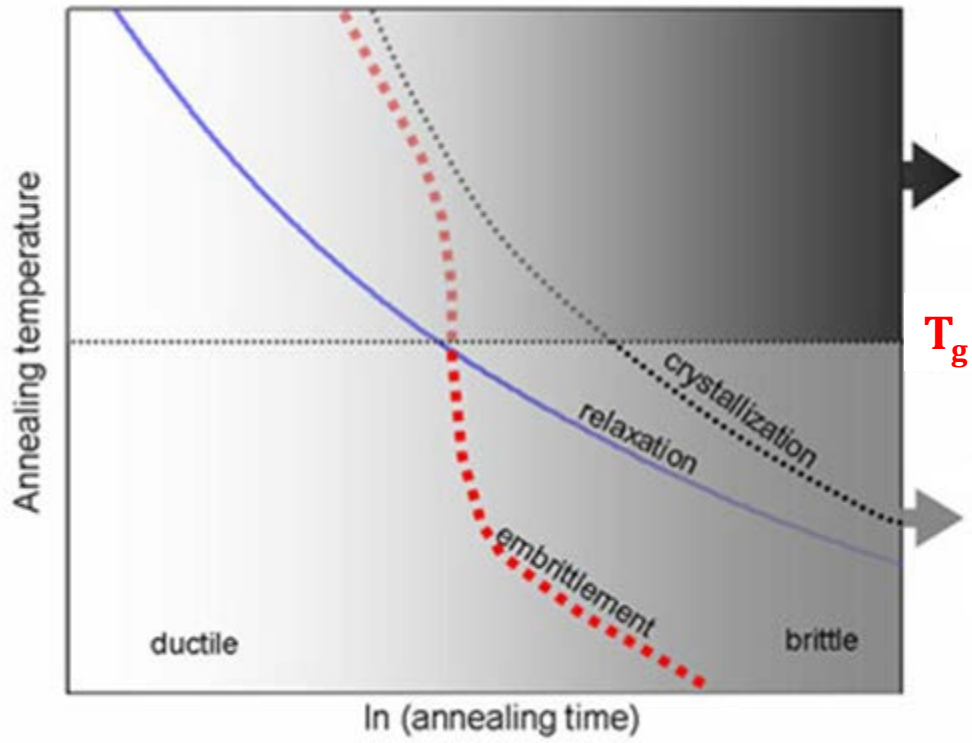

T_g

Embrittlement due to Crystallization

Embrittlement due to Relaxation

5

Crystallization Behavior

Temp. or Pressure ↓

Amorphous phase → crystal phase

(high E (metastable) state)

Tailor the microstructure to obtain a glass+nanocrystal or an ultrafine-grained composite, or a completely crystalline materials of different grain sizes by controlling the time and temperature of crystallization.

- Studies on the crystallization behavior of metallic glasses also provide an opportunity to study the kinetics of crystallization and also the micromechanisms of crystallization. Such results will provide a clear understanding of the way the metallic glass transforms into the crystalline state and offer a means to impede or control the crystallization behavior.

  → the mechanical and other properties could be optimized through a proper understanding of the crystallization behavior of metallic glasses.

- Any property of the material that changes on crystallization of the metallic glass may be used to monitor the crystallization behavior. These include electrical resistivity, saturation magnetization, magnetic coercivity, and elastic modulus, among others. When these properties are followed as a function of temperature during the heating of the metallic glass, there is a sharp and discontinuous change at the crystallization temperature. However, such methods are indirect and therefore caution should be exercised in using them to determine the kinetics of crystallization.

Crystallization → Change of Physical Properties

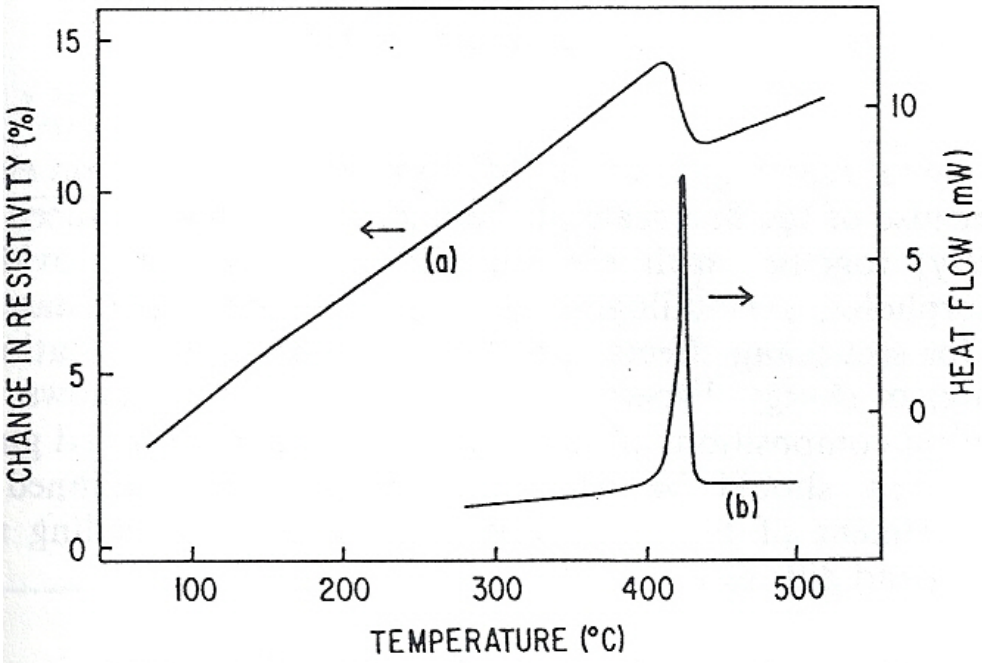

Figure 10.3 (a), Resistivity curve obtained by heating the glass $Fe_{40}Ni_{40}B_{20}$ at 5 K/min from room temperature (courtesy of J. Rout). (b), DSC trace obtained under the same conditions

→ Monitor the crystallization of metallic glass : electrical resistivity – sharp decrease in onset of crystallization

Any of the property changes described above may be used to monitor the crystallization of a metallic glass.

- Electrical Resistivity
- Elastic Modulus
- Magnetic coercivity
- Saturation magnetization

and so on.

Crystallization Behavior

Temp. or Pressure ↓

Amorphous phase → crystal phase

(high E (metastable) state)

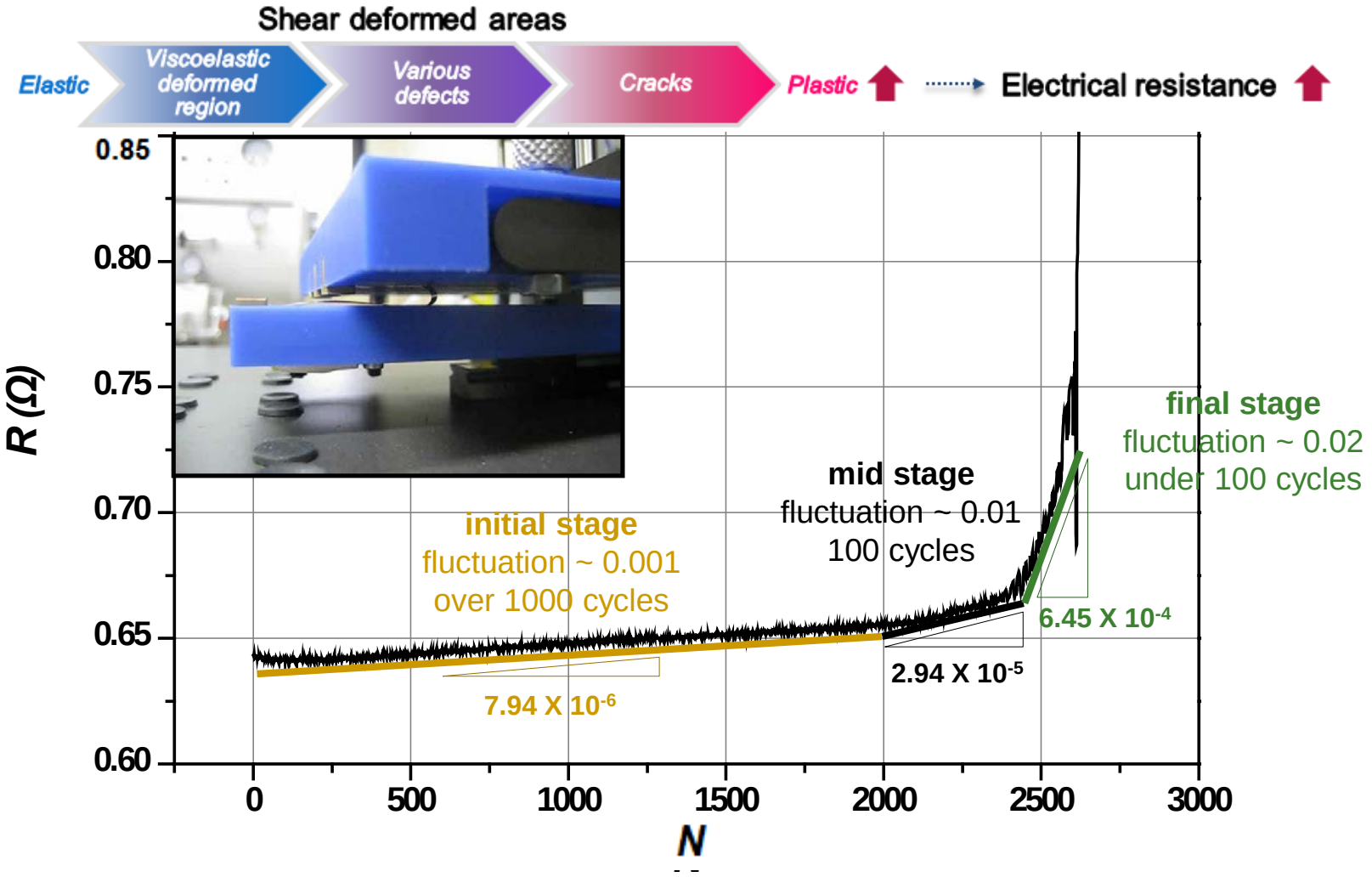

Measurement of resistance change during bending fatigue test of MG ribbons

CRYSTALLIZATION

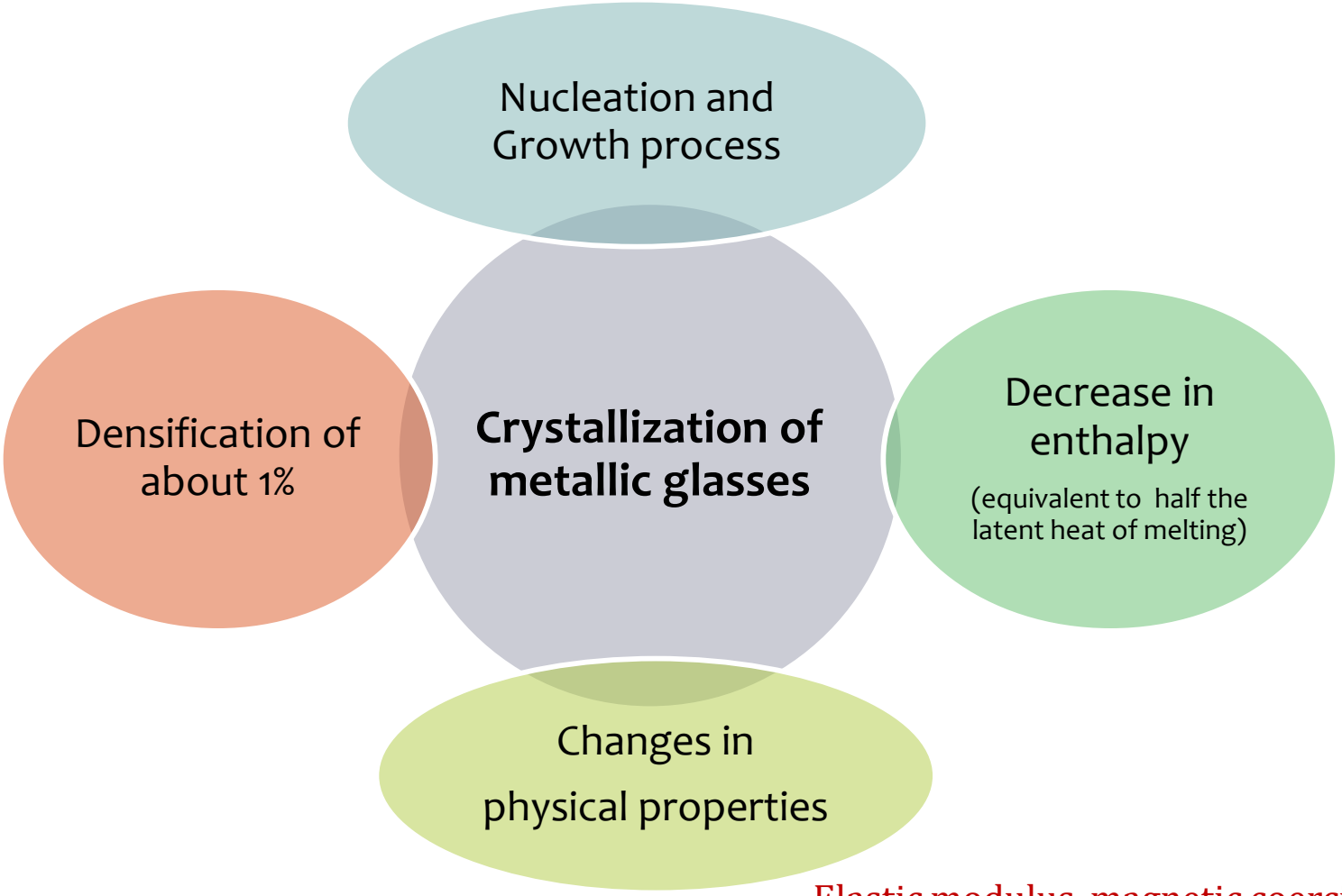

Elastic modulus, magnetic coercivity

5.2.3 Structural Details

- **Amorphous vs Nanocrystalline**

1) *Microstructural observation*

XRD, (HR)TEM, *EXAFS …*

2) *Thermal analysis*

DSC (Differential Scanning Calorimetry)

: Measure heat absorbed or liberated during heating or cooling

cf) **a) *glass*** → ***nucleation & growth***

(perfect random)

b) *local clustering*: quenched-in nuclei → ***only growth***

c) *Nanocrystalline* → ***growth***

X-ray or Neutron results

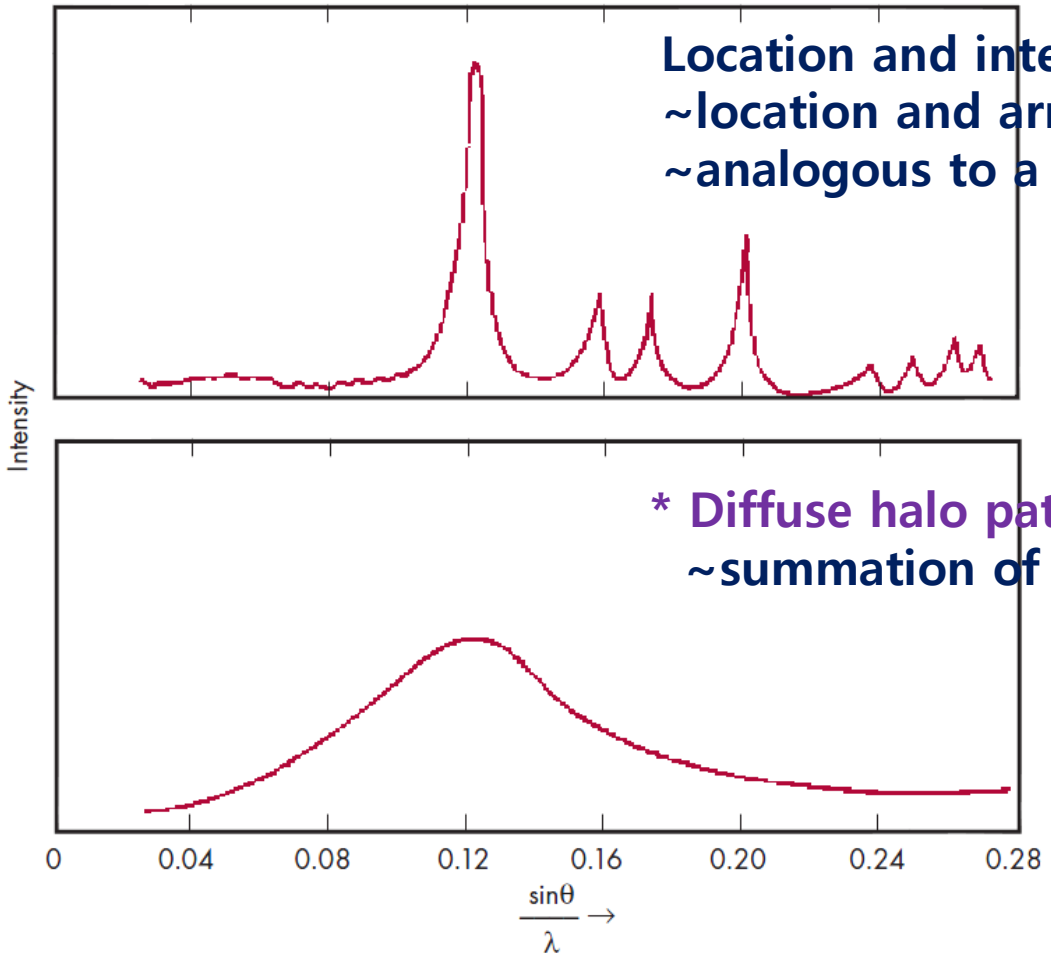

Location and intensity of peaks
~location and arrangement of atoms
~analogous to a fingerprint

*** Diffuse halo pattern**
~summation of interference

Figure 3. Characteristic Diffraction Patterns from Crystalline Material (Top) and Amorphous Material (Bottom).

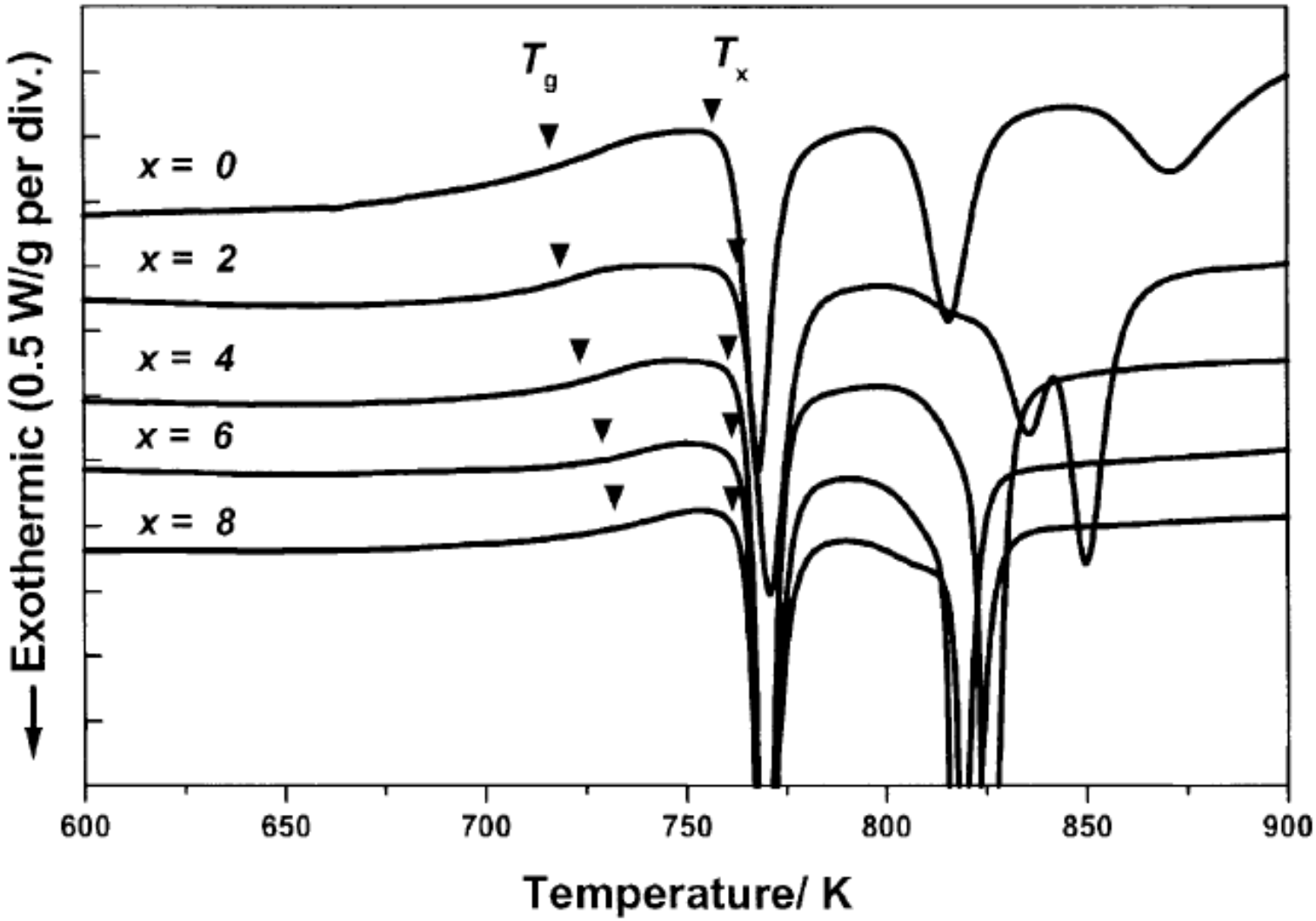

Fig. 1. DSC traces of rapidly solidified $Cu_{47}Ti_{33}Zr_{11}Ni_{8-x}Sn_xSi_1$ ($x = 0, 2, 4, 6, 8$) alloy ribbons obtained during heating with a heating rate 0.667 K/s.

< X-ray diffraction >

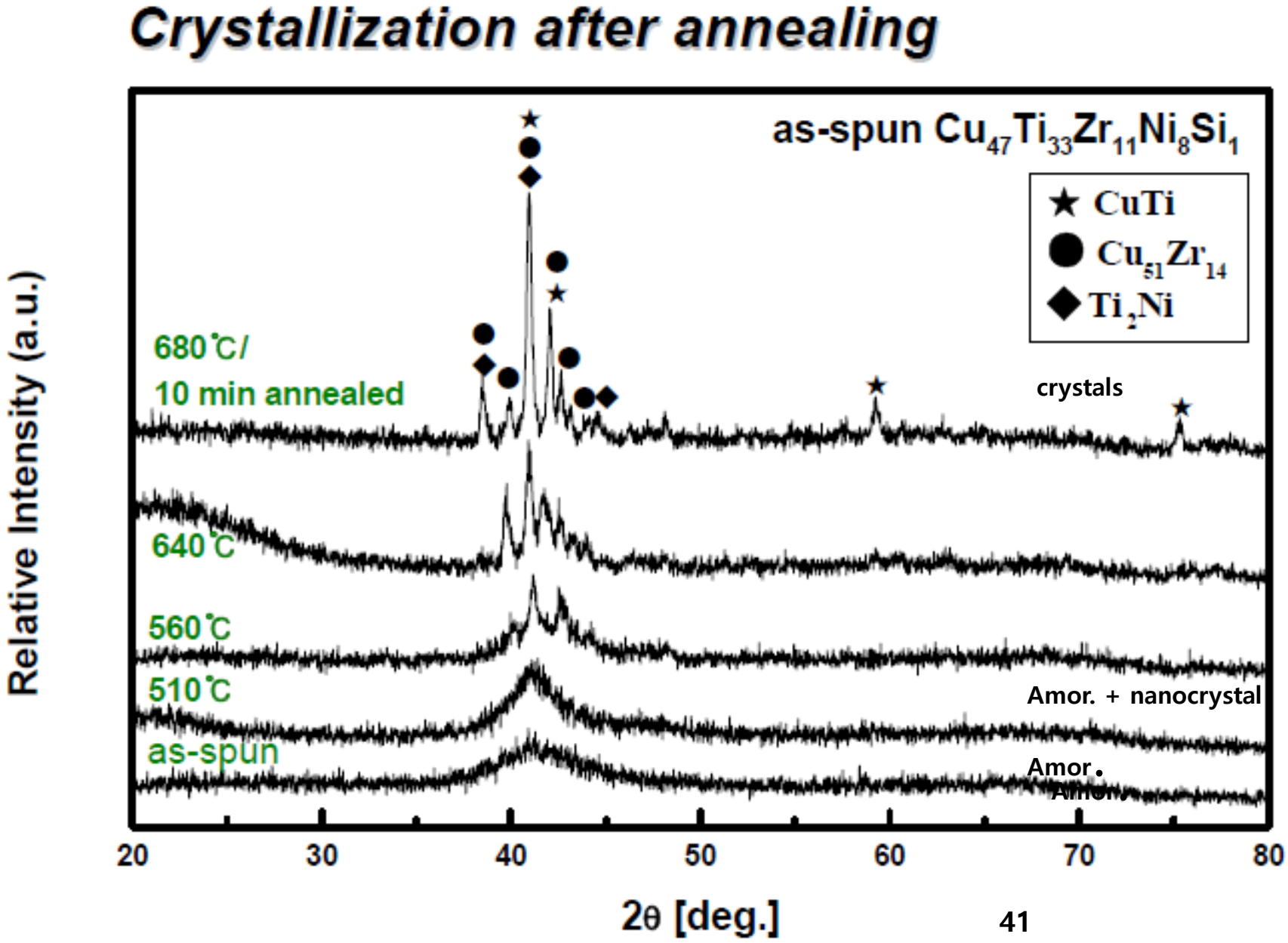

Electron Diffraction Pattern--Spot to Ring

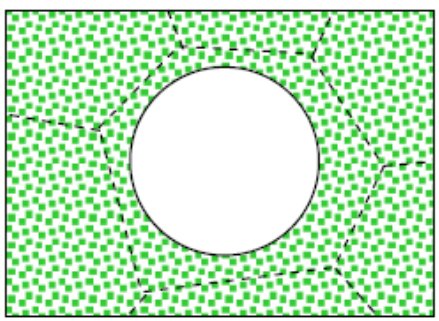

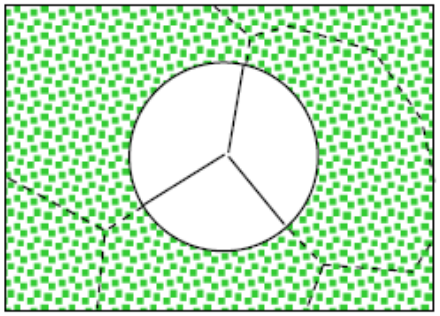

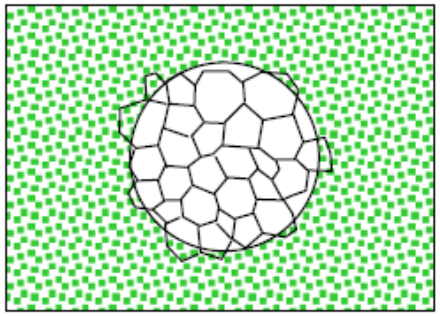

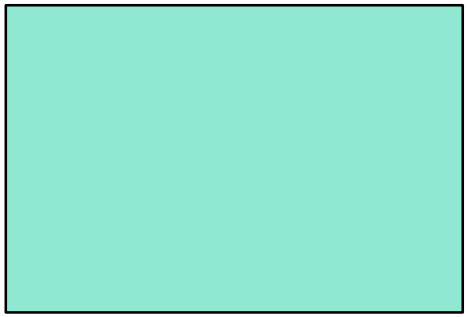

(a)

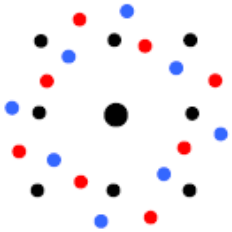

(b)

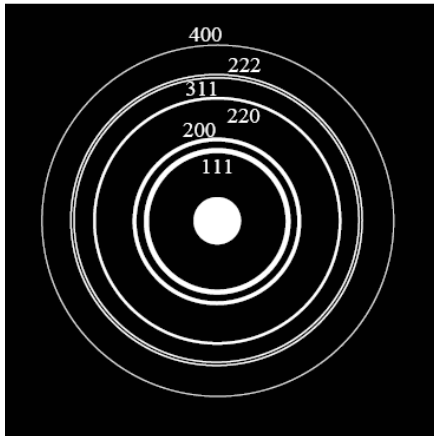

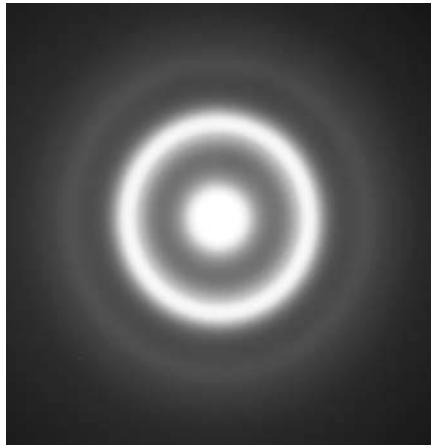

Selected area diffraction

$CoSi_x$ film on Si
after heat treatment
at 800 °C

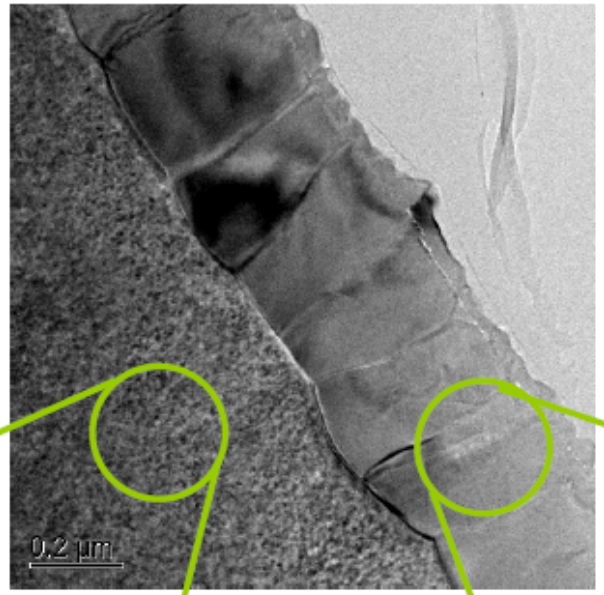

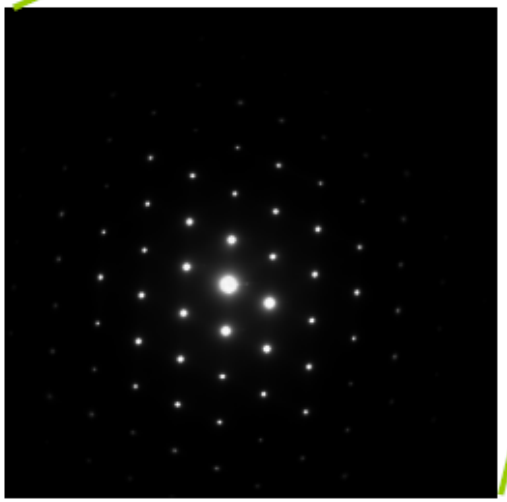

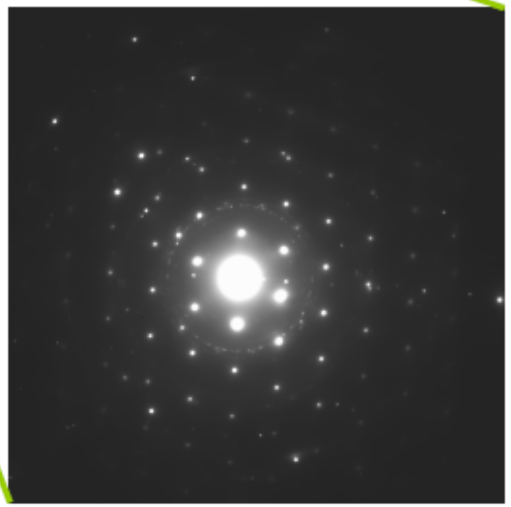

Formation of Cobalt Silicide by filter metal vacuum arc deposition
Y. Zhang, C.M. Wang, D.E. McCready
Pacific Northwest National Laboratory, Richland, WA 99352, USA
T. Zhang, Y. Wu
Institute of Low Energy Nuclear Physics, Beijing Normal University, Beijing, China
H.J. Whitlow[1]
Department of Physics University of Jyväskylä, Jyväskylä, Finland and
School of Technology and Society, Malmö högskola, Malmö, Sweden

Ring pattern

- Typical polycrystalline Au diffraction pattern

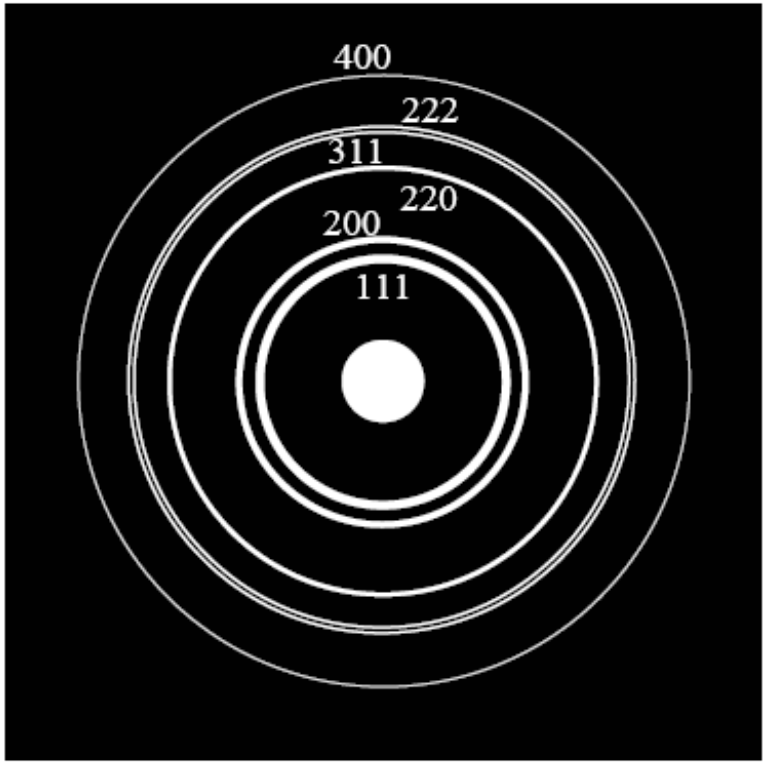

Amorphous materials

- Diffused ring pattern
- Reflecting the short range ordered structure
- Often seen at contamination layer or on carbon support film

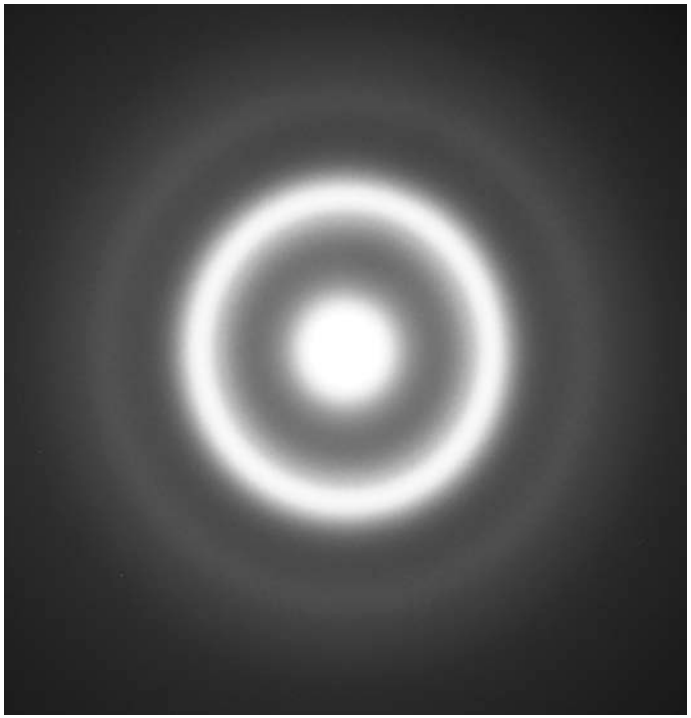

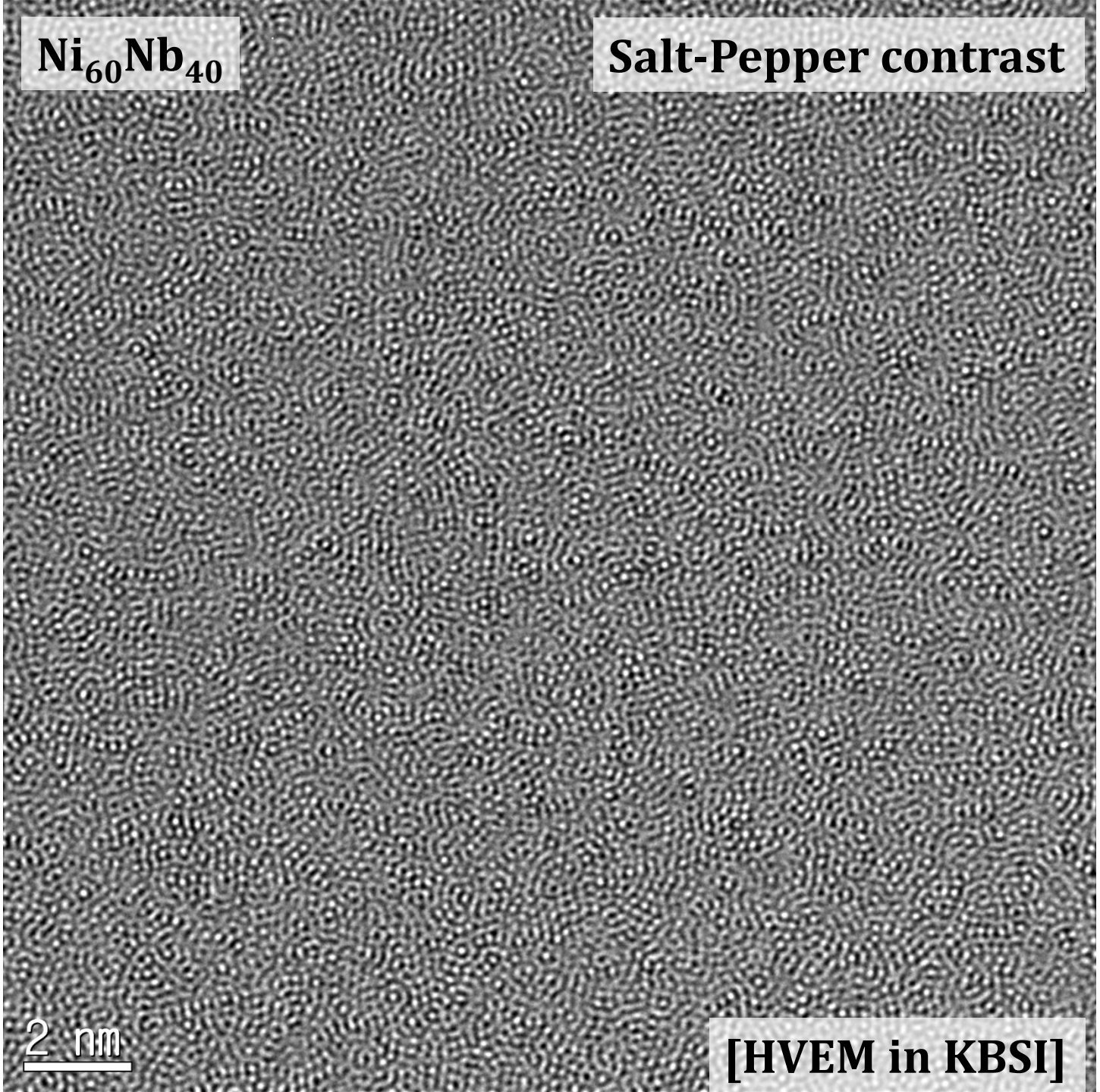
$Ni_{60}Nb_{40}$
Salt-Pepper contrast
2 nm
[HVEM in KBSI]

Structural analyses: HRTEM

$Cu_{46}Zr_{42}Al_7Y_5$

As-melt-spun

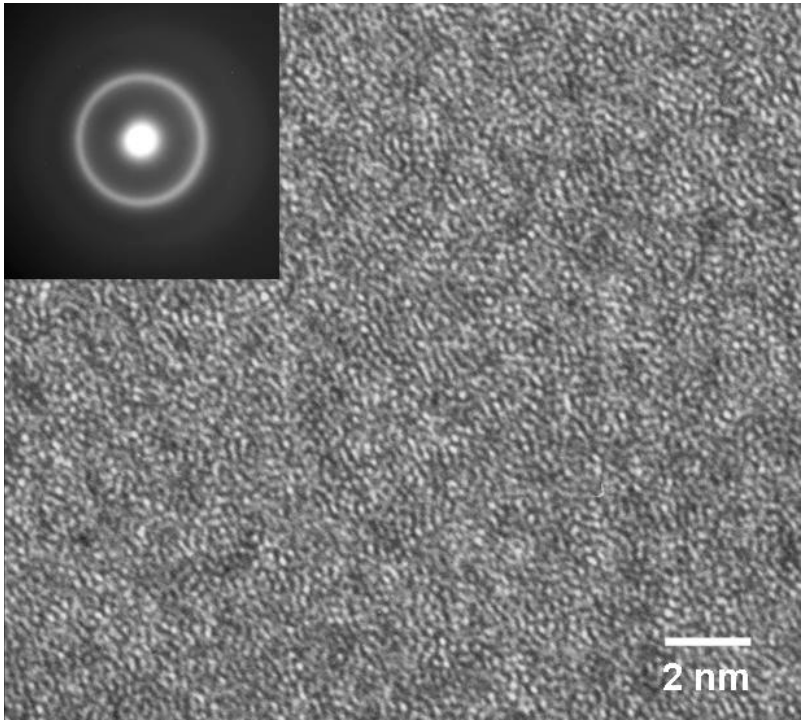

Heated up to 480℃

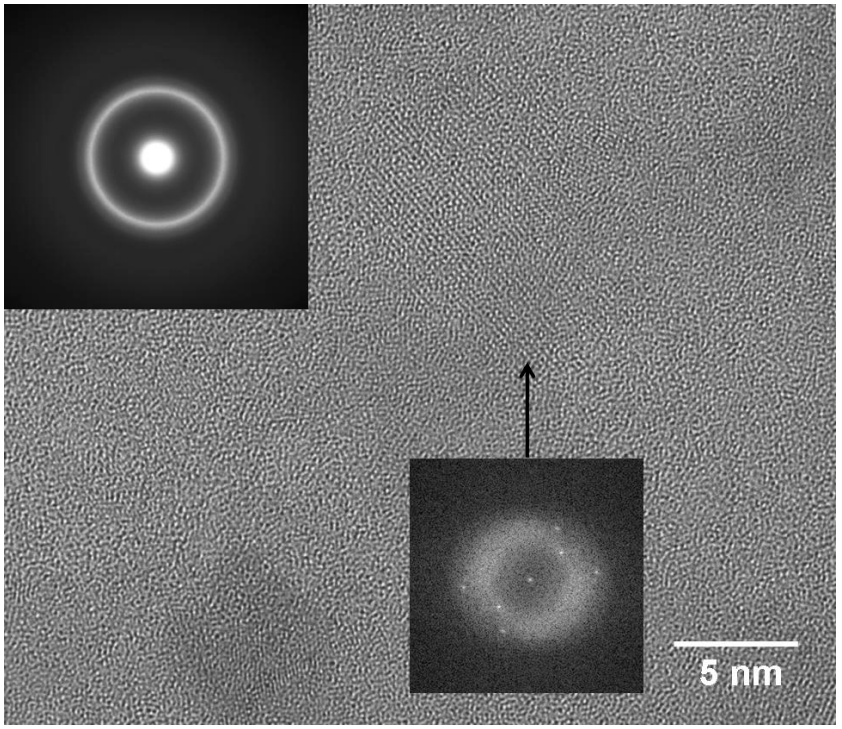

: nanocrystallization of Y rich amorphous phase due to relatively lower GFA

*** Acta Materialia, 54, 2597 (2006)**

TEM results for $Nd_{30}Zr_{30}Al_{10}Co_{30}$ alloy

$Nd_{60}Al_{10}Co_{30}$
2.91 Å

$Nd_{30}Zr_{30}Al_{10}Co_{30}$
2.37 Å, 2.99 Å

$Zr_{60}Al_{10}Co_{30}$
2.40 Å

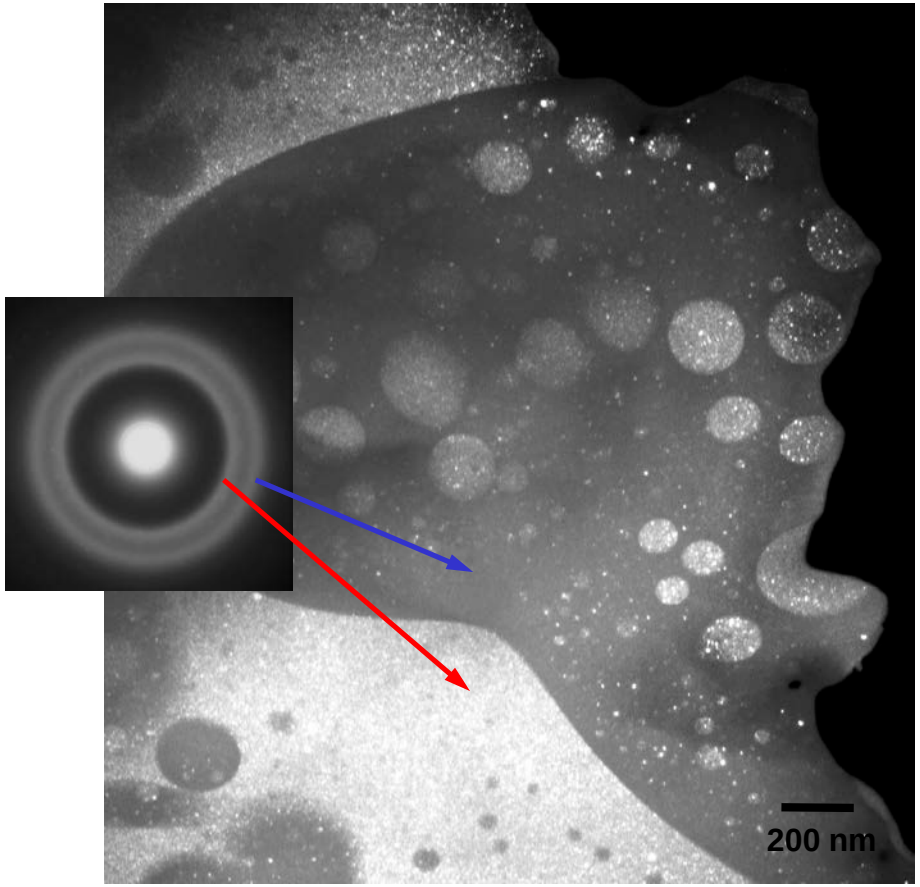

SADP and Dark-field TEM image

Angle range of Small angle scattering

- Length scale of small angle scattering : 1 – 1000 um

- Information on relatively large ***r*** is contained in ***I(q)*** at relatively small ***q (=4πsinθ/λ)***

- Bragg's law : ***sinθ=λ/2d***

d = few Å ***λ*** = 1 Å ***2θ*** = 20
d = 100 Å ***λ*** = 1 Å ***2θ*** = 0.6

- Sample contains a scattering length density inhomogeneity of dimension larger than 1 nm, scattering becomes observable in small angle region (0 ~ 4º)

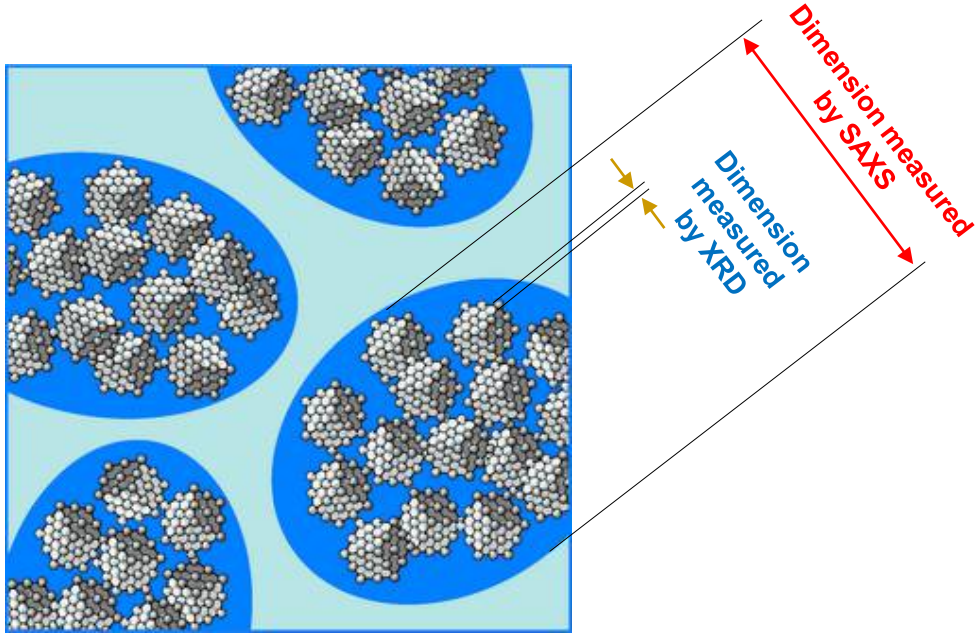

Diffraction v.s. Small angle scattering

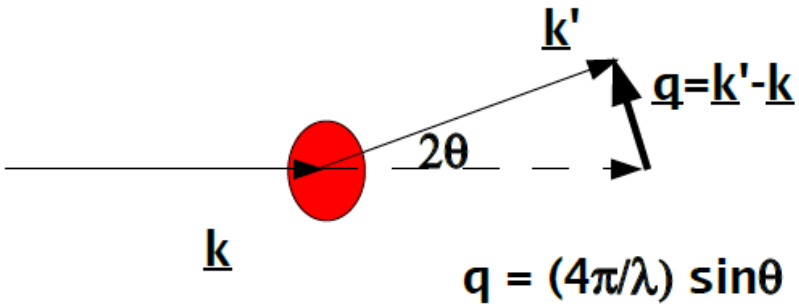

$q = (4\pi/\lambda)\sin\theta$

x-rays scatter from *electrons*

neutrons scatter from *nuclei* and *magnetic moments*

diffraction

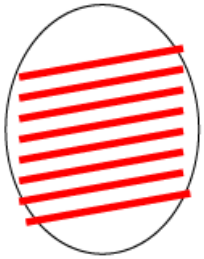

- scattering from *atomic structures*
- size of objects ~ λ
- small length scale -> large angle

small-angle scattering

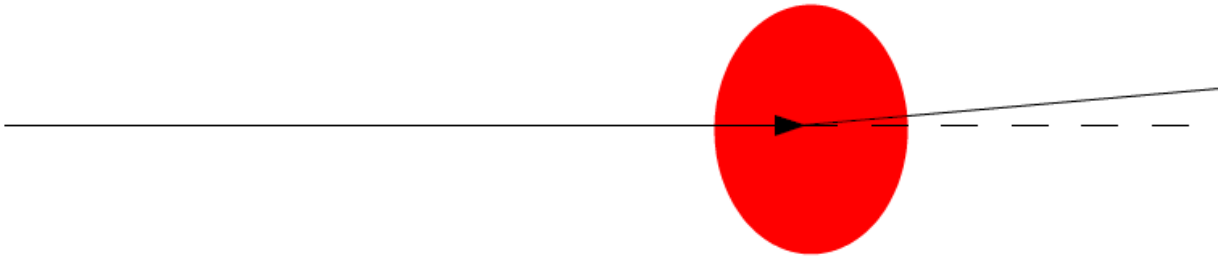

- scattering from *interfaces*
- size of objects >> λ
- large length scale -> small angle

Length scale for small angle scattering

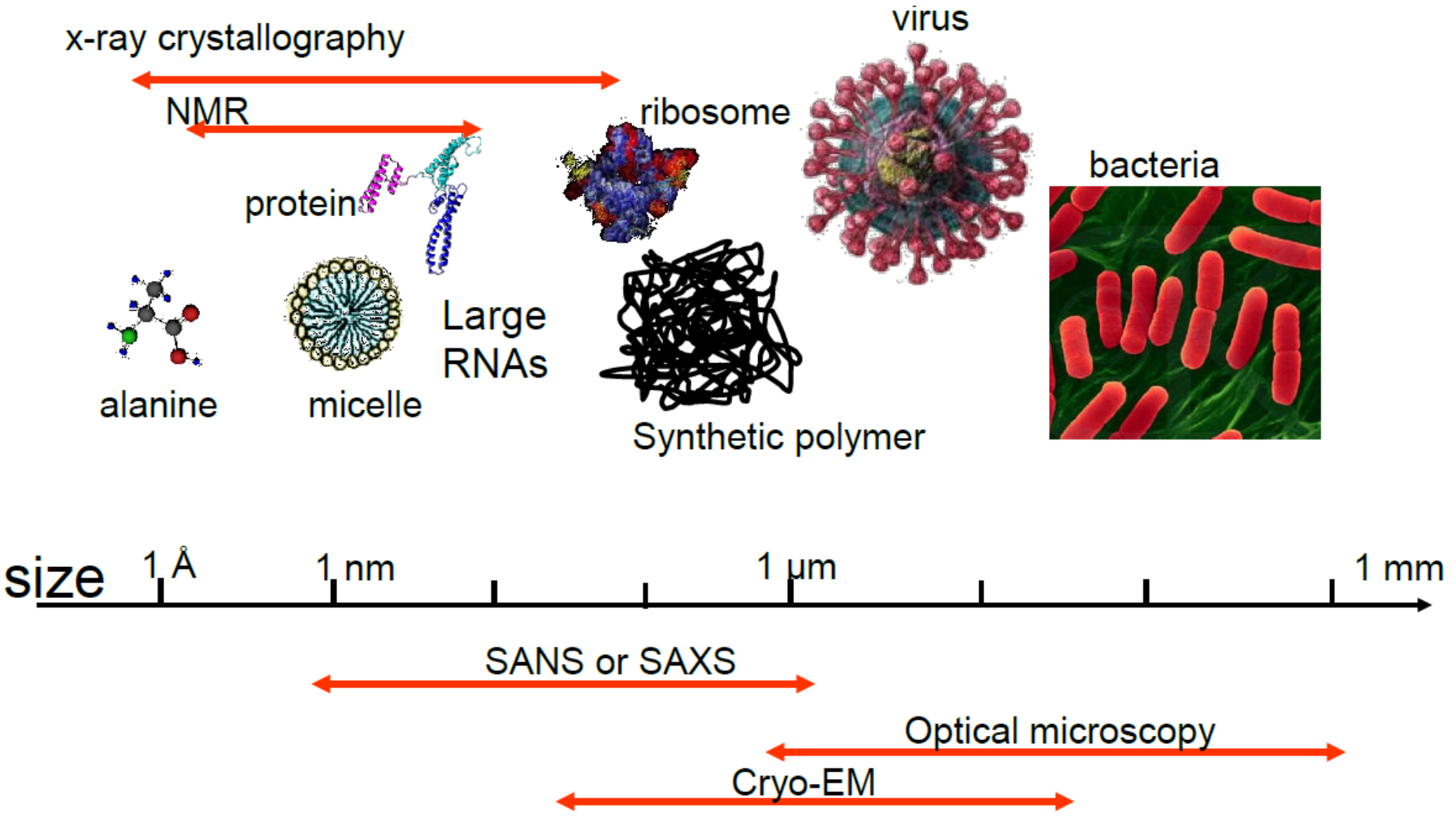

The scope of small angle X-ray scattering in terms of spatial dimension covers ~1nm to ~1μm ranges, perfectly suitable for biomolecular structrual study.

Scattering length density

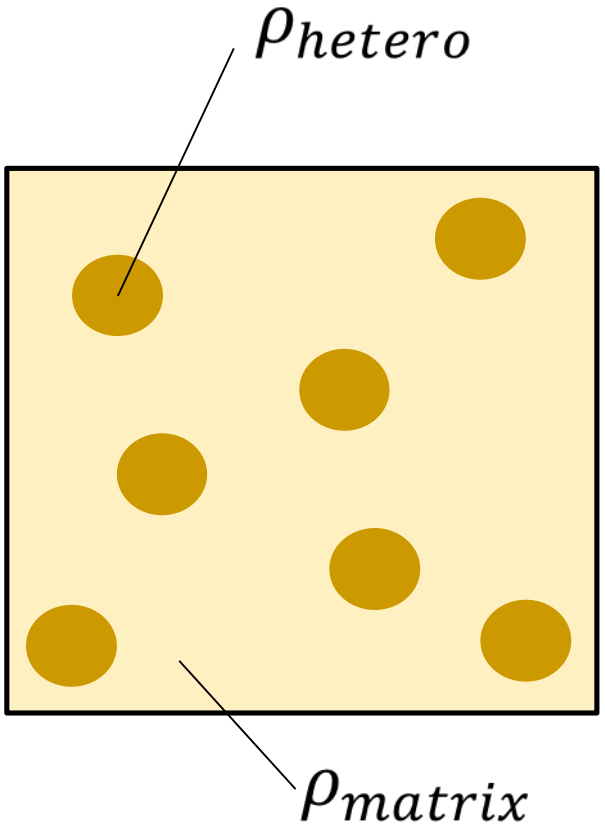

Scattering length density (of heterogeneities)

$$\rho = \frac{\sum_j^n b_j}{\bar{V}}$$

b_j : bound coherent scattering length of atom j

$\bar{V}$: Volume containing the n atoms

$$\Delta\rho = \rho_{hetero} - \rho_{matrix}$$

Intensity in small angle scattering

Scattering length density (of heterogeneities)

$$\rho = \frac{\sum_j^n b_j}{\bar{V}}$$

$$\Delta\rho = \rho_{hetero} - \rho_{matrix}$$

$$\bar{V} = \frac{M_w}{N_A \cdot \rho_{mass}}$$

$$I(q) = \Delta\rho^2 d_N \int_0^R N(r)[V(r)F(q,r)]^2 dr$$

d_N : number density factor
N(r) : normalized size distribution
V(r) : Volume
F(q,r) : Form factor of particles

$\Delta\rho = \rho_{hetero} - \rho_{matri}$

Common factors in both SANS and SAXS

Coherent and Incoherent Scattering

items	X-ray	neutron
source	collision of electrons with target metals(Cu, Mo, W…) acceleration of charged particles	nuclear reactor spallation neutron source (accelerator)
scattered by	electrons	atomic nuclei, unpaired spins
interaction	EM(electromagnetic)	Nuclear(strong int.) EM
scattering amplitude	linearly depend on Z	nearly indep. on Z
sample amount	μg ~ mg	~g
meas. time	$10^{1\sim2}$min (step scan: ~hr)	$10^{0\sim2}$ hr
hard to see	relatively light elements (H, Li, B, C, O …)	highly abs. nuclei (Gd, Sm, Eu, Cd, B…)

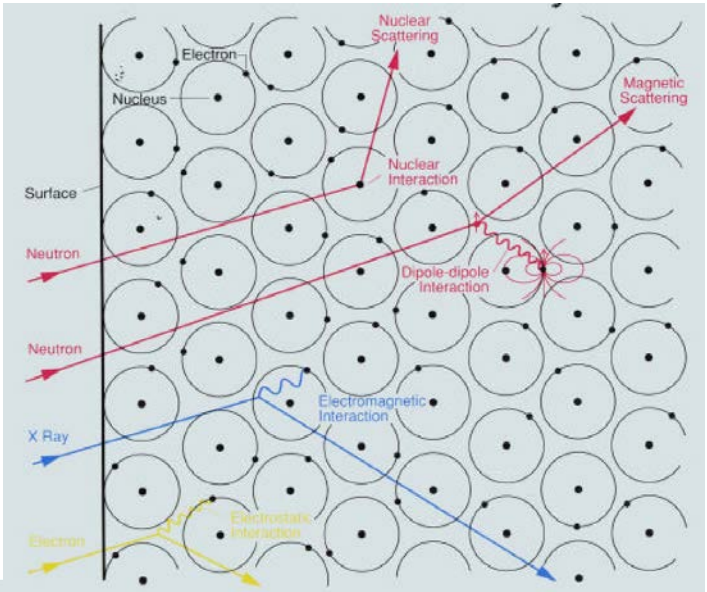

From the Roger Pynn's lecture

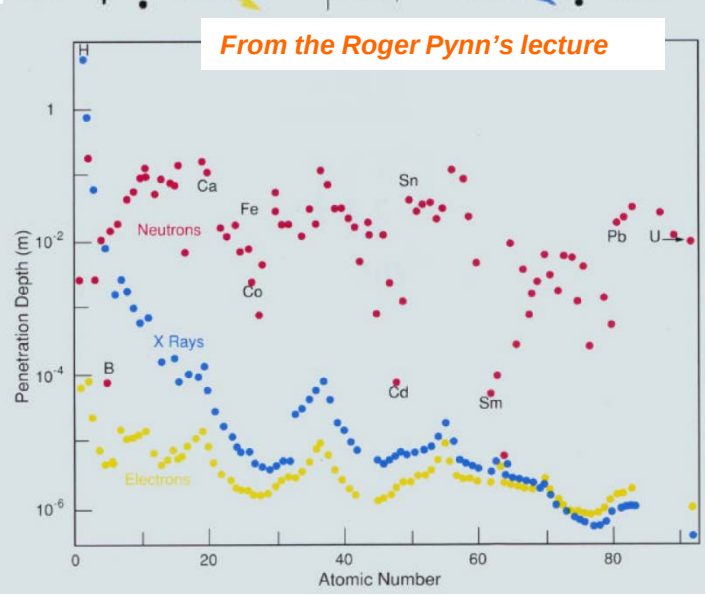

Neutron scattering length

$$\Psi = \psi_{in} + \psi_{scatt} = e^{i\,k\,z} - (b/r)\, e^{i\,k\,r}$$

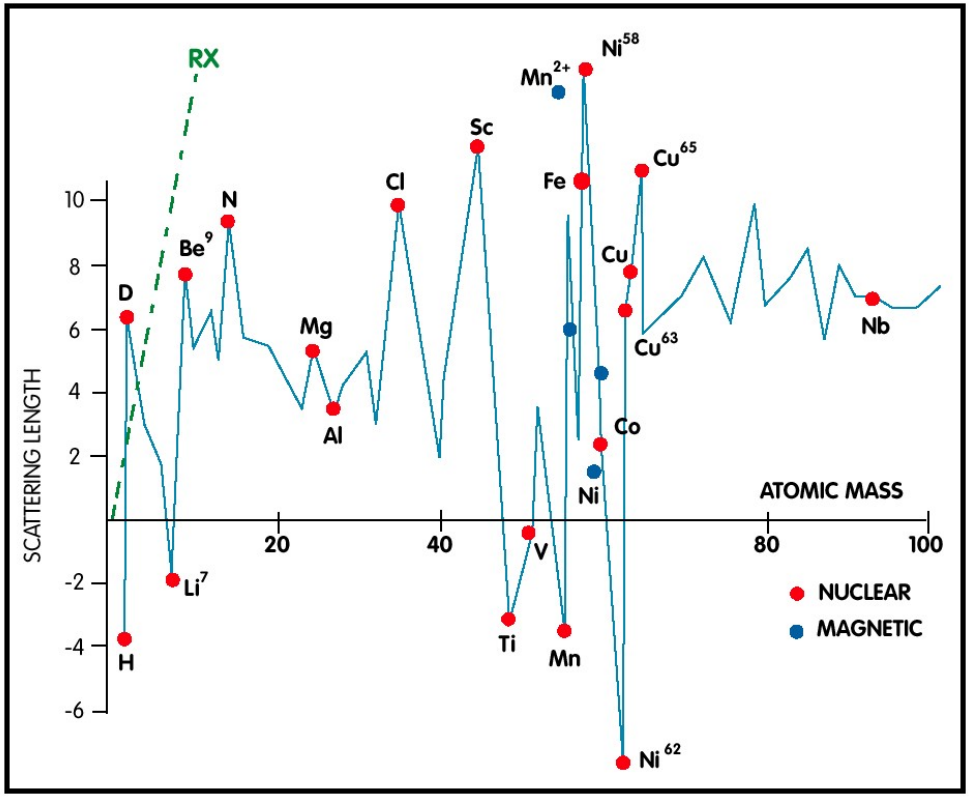

- **intrinsic property !!!**
- **order of 10^{-15}m (fm)**
- **sometimes negative or imaginary values (resonance scattering)**
- **independent of the thermal neutron energy**
- **no correlation with Z or A**